Cell Reports

Report

Hhex Directly Represses BIM-Dependent Apoptosis to Promote NK Cell Development and Maintenance

Graphical Abstract

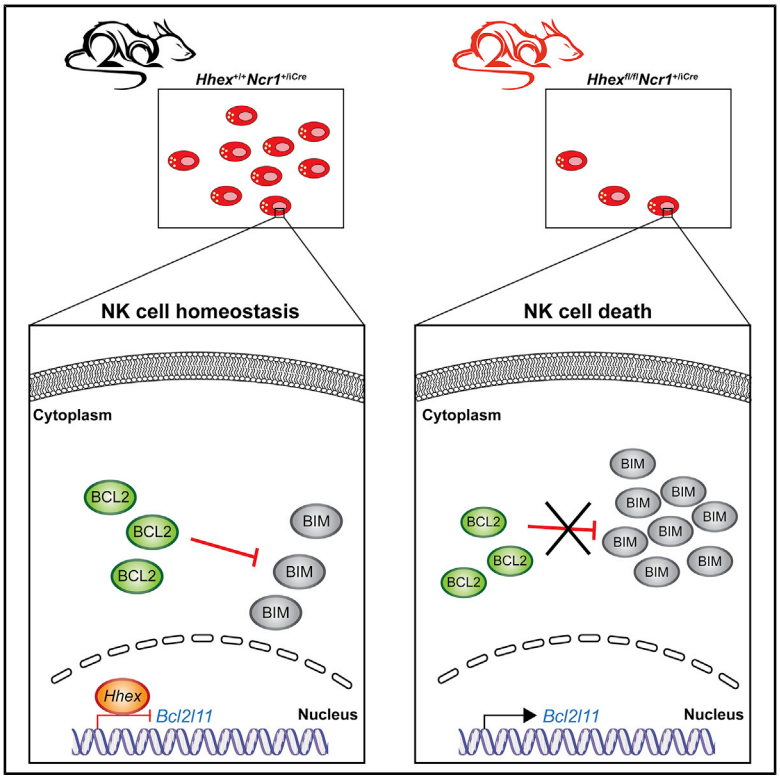

Highlights

- *Hhex* is continuously expressed during NK cell development
- Conditional deletion of *Hhex* leads to ~70% NK cell loss
- *Hhex* is a regulator of pro-apoptotic factor BIM (*Bcl2l11*) expression
- Simultaneous deletion of *Hhex* and *Bcl2l11* restores NK cell numbers

Authors

Wilford Goh, Sebastian Scheer, Jacob T. Jackson, ..., Matthew P. McCormack, Stephen L. Nutt, Nicholas D. Huntington

Correspondence

nicholas.huntington@monash.edu.au

In Brief

The role of *Hhex* in NK cells remains unclear, even though there is a strong correlation between *Hhex* expression and NK cell numbers. Using conditional knockout mouse models, Goh et al. establish *Hhex* as a critical regulator of NK cell development by preventing BIM-mediated NK cell death.

Goh et al., 2020, Cell Reports *33*, 108285
October 20, 2020
https://doi.org/10.1016/j.celrep.2020.108285

CellPress

Cell Reports

CellPress
OPEN ACCESS

Report

Hhex Directly Represses BIM-Dependent Apoptosis to Promote NK Cell Development and Maintenance

Wilford Goh,[1,2] Sebastian Scheer,[3] Jacob T. Jackson,[1,2] Soroor Hediyeh-Zadeh,[1] Rebecca B. Delconte,[1,2] Iona S. Schuster,[4,5] Christopher E. Andoniou,[4,5] Jai Rautela,[1,2,3,6] Mariapia A. Degli-Esposti,[4,5] Melissa J. Davis,[1,2,7] Matthew P. McCormack,[8] Stephen L. Nutt,[1,2] and Nicholas D. Huntington[1,2,3,6,9,*]

[1]The Walter and Eliza Hall Institute of Medical Research, Parkville, Victoria, 3052, Australia
[2]Department of Medical Biology, Faculty of Medicine, Dentistry and Health Sciences, The University of Melbourne, Melbourne, Victoria, 3010, Australia
[3]Department of Biochemistry and Molecular Biology, Biomedicine Discovery Institute, Monash University, Clayton, Victoria, 3800, Australia
[4]Centre for Experimental Immunology, Lions Eye Institute, Nedlands, Western Australia, 6009, Australia
[5]Department of Microbiology, Biomedicine Discovery Institute, Monash University, Clayton, Victoria, 3800, Australia
[6]oNKo-Innate Pty Ltd., 27 Norwood Cres, Moonee Ponds, Victoria, 3039, Australia
[7]Department of Clinical Pathology, Faculty of Medicine, Dentistry and Health Sciences, The University of Melbourne, Melbourne, Victoria, 3010, Australia
[8]The Australian Centre for Blood Diseases, Monash University, Melbourne, Victoria, 3004, Australia
[9]Lead Contact
*Correspondence: nicholas.huntington@monash.edu.au
https://doi.org/10.1016/j.celrep.2020.108285

SUMMARY

Hhex encodes a homeobox transcriptional regulator important for embryonic development and hematopoiesis. *Hhex* is highly expressed in NK cells, and its germline deletion results in significant defects in lymphoid development, including NK cells. To determine if *Hhex* is intrinsically required throughout NK cell development or for NK cell function, we generate mice that specifically lack *Hhex* in NK cells. NK cell frequency is dramatically reduced, while NK cell differentiation, IL-15 responsiveness, and function at the cellular level remain largely normal in the absence of *Hhex*. Increased IL-15 availability fails to fully reverse NK lymphopenia following conditional *Hhex* deletion, suggesting that *Hhex* regulates developmental pathways extrinsic to those dependent on IL-15. Gene expression and functional genetic approaches reveal that *Hhex* regulates NK cell survival by directly binding *Bcl2l11* (Bim) and repressing expression of this key apoptotic mediator. These data implicate *Hhex* as a transcriptional regulator of NK cell homeostasis and immunity.

INTRODUCTION

Natural killer (NK) cells are innate lymphocytes best known for their functional efficacy against transformed and virus-infected cells. With growing interest in the use of NK cells as immunotherapeutic agents (Huntington et al., 2020), the need for a deeper understanding of basic NK cell biology has emerged. Much effort has been channeled into understanding the regulation of transcriptional programs specific to NK cells and how this process influences NK cell development and function (Goh and Huntington, 2017; Sun, 2016). Recent studies have provided further mechanistic insights on how ID2 (Zook et al., 2018; Delconte et al., 2016b) and NFIL3 (Kostrzewski et al., 2018) regulate NK cell development. Deletion of another transcription factor, TCF1, revealed a correlation between granzyme expression and both NK cell maturation and function (Jeevan-Raj et al., 2017). Other transcription factors, such as FOXO3, CBFB, RUNX1, RUNX3, and IRF8, have also been implicated in NK cell responses against viral infections (Adams et al., 2018). T-bet was found to be specifically required for the persistence of MCMV-specific memory NK cells, revealing stage-specific requirements for T-bet and Eomes during a viral response (Madera et al., 2018). Finally, close links between cellular metabolism and NK cell homeostasis, maturation, proliferation, and function (Marçais et al., 2013; Donnelly et al., 2014; Yang et al., 2016; Ali et al., 2015) have led to the identification of transcriptional regulators of NK cell metabolism. Three transcription factors, SREBP (Assmann et al., 2017), c-Myc (Loftus et al., 2018), and RFX7 (Castro et al., 2018), have been implicated thus far, though more may be added to this group of transcription factors as studies begin to re-examine transcription factors in NK cell metabolism.

Hhex (hematopoietically expressed homeobox) is a member of the Homeobox family of transcription factors (Bedford et al., 1993; Crompton et al., 1992; Ghosh et al., 1999; Hromas et al., 1993). Like other homeodomain-containing transcription factors (Gehring, 1987), *Hhex* is a critical regulator of cell differentiation and morphogenesis, particularly during embryonic development, when it is highly expressed in the developing liver, thyroid, and lungs (Bogue et al., 2000; Keng et al., 1998; Thomas et al., 1998). *Hhex*-deficient mouse embryos fail to survive beyond mid-gestation because of severe liver, forebrain, thyroid, and

cardiovascular malformation (Hallaq et al., 2004; Keng et al., 2000; Martinez Barbera et al., 2000). *Hhex* is also required for development of the various hematopoietic lineages, albeit to varying extents. Erythroid progenitors and erythrocytes develop independently of *Hhex*, whereas *Hhex* is only required for myeloid development in times of hematopoietic stress (Guo et al., 2003; Kubo et al., 2005; Paz et al., 2010; Goodings et al., 2015; Jackson et al., 2015, 2017). *Hhex* dependency during lymphoid development is best understood in the context of B cells that express the highest levels of *Hhex* among the lymphoid lineages (Bedford et al., 1993; Goodings et al., 2015; Heng et al., 2008; de Graaf et al., 2016). *Hhex*-deficient mice lack mature B cells because of impaired IL-7 signaling, dysregulated expression of cell cycle genes, increased apoptosis, and developmental arrests of early progenitors (Jackson et al., 2015; Goodings et al., 2015). The few remaining B cells were also reported to be defective for antibody production and immunoglobulin receptor arrangement (Bogue et al., 2003). Similarly, defective T cell development in the absence of *Hhex* has also been observed, though only in a competitive transplantation setting (Jackson et al., 2015), as T cells express much lower levels of *Hhex* compared with B and NK cells (Bedford et al., 1993; Goodings et al., 2015; Heng et al., 2008; de Graaf et al., 2016).

Hhex has also been implicated in the development of NK cells with comparable *Hhex* expression as B cells (de Graaf et al., 2016; Heng et al., 2008), as significant NK cell losses were observed in chimeric studies with germline-deficient mice (Jackson et al., 2015). However, whether this deficiency resulted from impaired lymphoid progenitor development or a role for *Hhex* later in NK cell development remains unclear. To address this question, we generated a mouse model that facilitates the inactivation of *Hhex* in NK cells. We find that *Hhex* is intrinsically required for homeostatic maintenance of lineage-committed NK cells and critical for promoting NK cell survival by repression of the pro-apoptotic factor BIM.

RESULTS AND DISCUSSION

Conditional Deletion of *Hhex* Leads to Significant NK Cell Loss

The role of *Hhex* in NK cell development and function remains enigmatic even though it is consistently expressed throughout NK differentiation (Figures 1A and S1A), and homozygous germline deletion of *Hhex* leads to a dramatic loss of NK cells *in vivo* (Jackson et al., 2015). Consequently, we generated $Hhex^{fl/fl}Ncr1^{+/Cre}$ mice to examine the role of *Hhex* within the NK cell lineage. Exons 2 and 3, which encode the homeodomain of *Hhex*, were targeted for *Cre*-mediated deletion in all NKp46-expressing cells so as to inactivate the transcriptional activity of *Hhex* in predominantly NK cells (Narni-Mancinelli et al., 2011). Appreciable loss of HHEX was observed by western blotting of NK cell lysates from $Hhex^{fl/fl}Ncr1^{+/Cre}$ mice (hereafter referred to as $Hhex^{\Delta/\Delta}$ mice; Figure 1B). Flow cytometric analysis of $CD3^{-}NK1.1^{+}NKp46^{+}$ NK cells revealed a striking loss in the proportion and total numbers of NK cells in the spleens (Figure 1C), bone marrow, and lungs (Figure S1B) of $Hhex^{\Delta/\Delta}$ mice. Therefore, *Hhex* plays a non-redundant role in the development and maintenance of lineage-committed NK cells. Although *Hhex* is well known for its regulatory role in cell development (Soufi et al., 2006; Hallaq et al., 2004; Hunter et al., 2007), NK cell maturation as defined by CD27 and CD11b expression (Figure 1D; Chiossone et al., 2009; Hayakawa and Smyth, 2006; Huntington et al., 2007b; Kim et al., 2002) was largely normal in $Hhex^{\Delta/\Delta}$ mice, barring minor differences among the immature and M2 subsets. In light of consistent *Hhex* expression during NK cell maturation and even NK cell loss across all maturation subsets, *Hhex* is likely to be continuously required by all differentiated NK cell subsets.

Loss of *Hhex* Does Not Alter NK Functionality *In Vitro*

To address the role of *Hhex* in NK cell function, we first examined the impact of *Hhex* deficiency on NK cell receptor expression, as functionality can be influenced by signals from activating and inhibitory receptors expressed on the cell surface (Morvan and Lanier, 2016). $Hhex^{\Delta/\Delta}$ mice possessed fewer NK cells expressing activating (Figure 1E) and inhibitory (Figure S1C) receptors of the Ly49 family. Expression of two other activating receptors, NKG2D and DNAM-1 (encoded by *Cd226*), was, however, significantly upregulated in the absence of *Hhex* (Figure 1F). Despite the changes in receptor expression, NK cell function remained intact, as similar proportions of IFN-γ producing or degranulating ($CD107a^{+}$) *Cre* control and $Hhex^{\Delta/\Delta}$ NK cells were observed after *ex vivo* stimulation with PMA/ionomycin, IL-12/IL-18, or plate-bound monoclonal antibodies against various activating receptors (Figure 1G). Genes encoding the IL-12 and IL-18 receptor subunits were also expressed at similar levels in *Cre* control and $Hhex^{\Delta/\Delta}$ NK cells (Figure S1D), suggesting intact recognition of IL-12 and IL-18. Finally, comparable rates of calcein release were measured when *Cre* control or $Hhex^{\Delta/\Delta}$ NK cells were incubated with B16F10 melanomas at various effector-to-target (E:T) ratios (Figure 1H), suggesting normal tumor killing on a per cell basis in the absence of *Hhex*. Overall, the data suggest that NK cell function is largely independent of *Hhex*.

Loss of *Hhex* Affects NK Cell and ILC1 Differentiation

To determine the underlying molecular phenotype of $Hhex^{\Delta/\Delta}$ NK cells, we performed RNA sequencing (RNA-seq) and identified a total of 690 differentially expressed genes (DEGs; false discovery rate [FDR] < 0.05; Figure 2A). The larger proportion of upregulated DEGs (401) suggests that *Hhex* functions predominantly as a transcriptional repressor, which is consistent with findings from other cell types (Paz et al., 2010; Guiral et al., 2001). Intriguingly, 68 of the 690 DEGs have previously been annotated as ILC1 signature genes (Robinette et al., 2015; Weizman et al., 2017; Seillet et al., 2016). NK cells ($CD49a^{-}CD49b^{+}$), DP cells ($CD49a^{+}CD49b^{+}$), and ILC1s ($CD49a^{+}CD49b^{-}$) make up cell types of the group 1 ILC compartment, and a degree of plasticity between the lineages has been proposed (Gao et al., 2017). Further testing against microarray data for splenic $CD127^{+}$ ILC1s and $CD127^{-}$ NK cells (Robinette et al., 2015) confirmed significant enrichment of ILC1 signature genes in $Hhex^{\Delta/\Delta}$ NK cells ($p = 0.001$; Figure 2B), including *Cxcr6*, a core ILC1 signature gene (Figure S2A). These data suggest that *Hhex* functions as a transcriptional repressor of ILC1 identity in NK cells. Additionally, gene set testing against KEGG pathways revealed a significant enrichment of cell cycle genes (FDR = 0.018) in $Hhex^{\Delta/\Delta}$

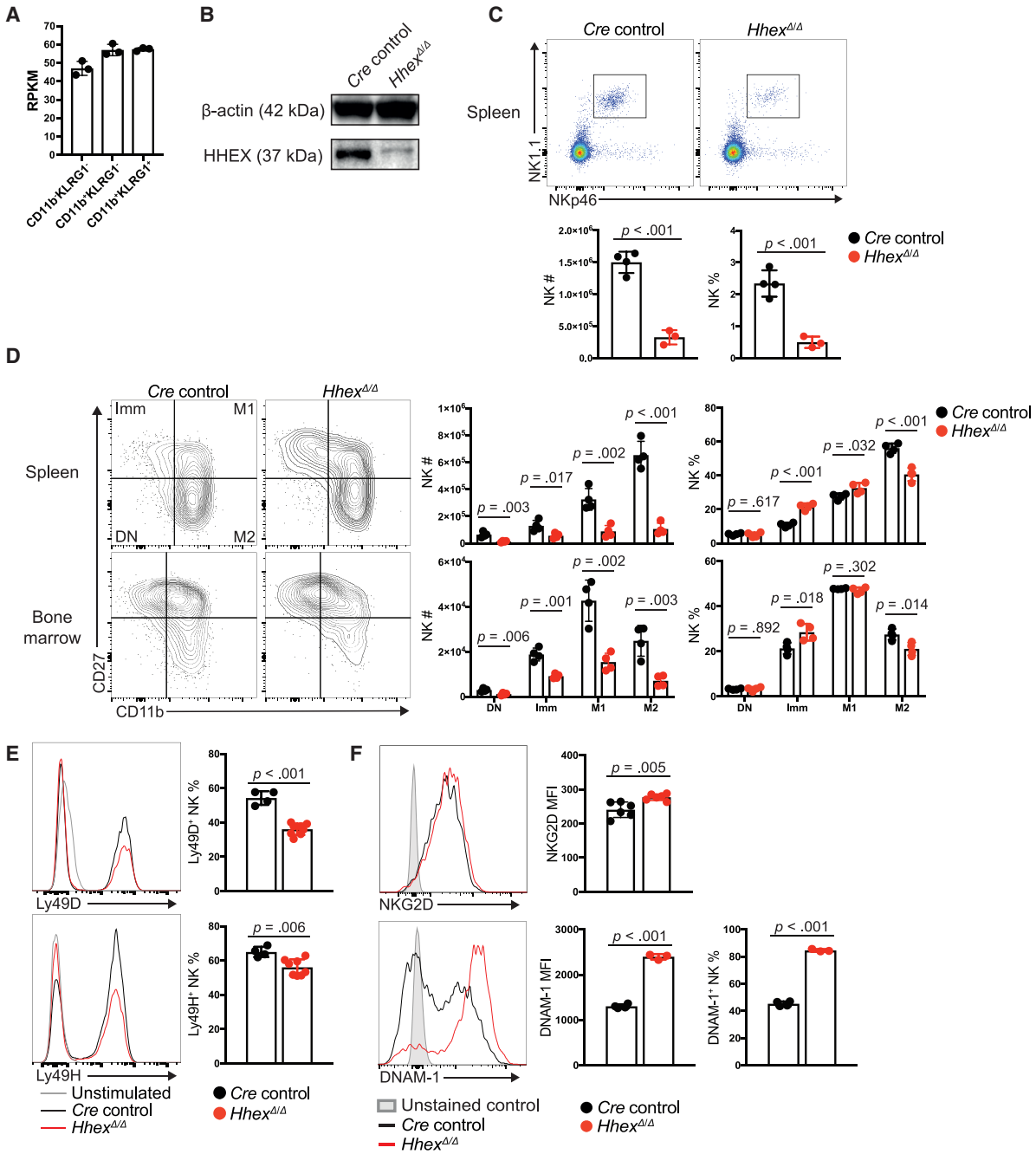

(legend on next page)

NK cells, most of which appear to be transcriptionally repressed by *Hhex*, but not genes associated with apoptosis, JAK/STAT signaling, and NK cell mediated cytotoxicity (Figure S2B).

Consistent with the significant increase in *Itga1* (gene encoding CD49a) mRNA transcripts in splenic $Hhex^{\Delta/\Delta}$ NK cells, we detected a significant increase in numbers and proportion of $CD49a^{+}CD49b^{+}$ DP cells not typically present in the spleen (Figure 2C), with similar trends in the bone marrow and liver (Figure S2C). ILC1 numbers were largely unaffected by the loss of *Hhex*, even though it is equally highly expressed in both NK cells and ILC1s (Figure S2D) and *Ncr1*-mediated *Hhex* deletion would also be predicted to occur in ILC1s. Despite the role for *Hhex* in repressing ILC1 gene expression, NK cells remained the predominant cell type (~70%) within the group 1 ILC compartment, and no differences in *Eomes* expression were detected by RNA-seq (Figure 2D). Flow cytometric analysis revealed a significant increase in the proportion of $CD49a^{+}CD49b^{+}$ DP cells that lacked EOMES (Figure 2E), suggesting acquisition of an ILC1-like phenotype following *Hhex* deletion. A possible explanation could be increased activin-A signaling, which induces an ILC1-like phenotype in NK cells (Gao et al., 2017; Rautela et al., 2019), as a result of augmented expression of *Acvr2a* (gene encoding activin receptor type-2A; Figure 2A) in $Hhex^{\Delta/\Delta}$ NK cells. In contrast, $CD49a^{-}CD49b^{+}$ $Hhex^{\Delta/\Delta}$ NK cells retained high Eomes and CD62L but low CD200R expression (Figure 2F; Weizman et al., 2017; Wang et al., 2018; Ng et al., 2018), which further validates their identity as bona fide NK cells. Thus, the significant enrichment of ILC1 signature genes within the $NKp46^{+}$ compartment of $Hhex^{\Delta/\Delta}$ mice stemmed from increased frequencies of $CD49a^{+}CD49b^{+}$ DP cells rather than increased expression of ILC1 signature gene expression among conventional NK cells.

Increased NK Cell Turnover in the Absence of *Hhex* that Is Not Driven by IL-15

Previous studies have reported impaired IL-7 signaling and attenuated IL-7Rα expression in *Hhex*-deficient B cells (Jackson et al., 2015; Goodings et al., 2015). Given that IL-7 and IL-15 both use the common γ chain receptor subunit (Noguchi et al., 1993; Carson et al., 1994; Sugamura et al., 1995) and share similar signaling pathways (Lin et al., 1995), we hypothesized that the drastic loss of NK cells in $Hhex^{\Delta/\Delta}$ mice could be due to impaired responses to IL-15, a key mediator of NK cell homeostasis (Kennedy et al., 2000; Cooper et al., 2002; Huntington et al., 2009). Despite similar expression of the IL-15 receptor subunits IL-15Rα (CD215), IL-15Rβ (CD122), and common γ chain (CD132) between *Cre* control and $Hhex^{\Delta/\Delta}$ NK cells (Figures 3A and S3A), Ki-67 expression was significantly higher in $Hhex^{\Delta/\Delta}$ NK cells but not the DP population (Figure 3B). The increase in NK cell turnover was confirmed by measuring EdU incorporation (Figure S3B). Consistent with increased NK cell turnover *in vivo*, $Hhex^{\Delta/\Delta}$ NK cells exhibited greater CTV dilution *in vitro* when cultured in ≥12.5 ng/mL rhIL-15 (Figure S3C) but ultimately failed to accumulate in greater numbers than *Cre* control NK cells (Figure 3C). Taken together, these data indicate that NK cells become hyper-proliferative in the absence of *Hhex*, but this results in a net loss rather than an accumulation of NK cells.

To further determine if the loss of NK cells in $Hhex^{\Delta/\Delta}$ mice could be due to aberrant JAK/STAT signaling events downstream of the IL-15 receptor, we assessed hematopoietic and NK cell reconstitution in mixed bone marrow chimeras generated with congenic $CD45.1^{+}$ control (wild-type [WT]) donors and $Hhex^{+/fl}$, $Hhex^{+/fl}caStat5b^{T/+}$, $Hhex^{-/\Delta}$, or $Hhex^{-/\Delta}caStat5b^{T/+}$ experimental donors (Figure 3D). Consistent across both hematopoietic and NK cell compartments, enforced IL-15 signaling via constitutive expression of the *Stat5b* transgene expression failed to prevent cell loss in the absence of *Hhex* (Figure 3E). Intact signal transduction via STAT5 was verified by comparing fold induction of phosphorylated STAT5 (pSTAT5) in *Cre* control and $Hhex^{\Delta/\Delta}$ NK cells following *in vitro* re-exposure to rhIL-15, which yielded only mild differences (Figure S3D). Other IL-15 signal transduction pathways, such as the PI3K/AKT/mTOR (Marçais et al., 2013; Donnelly et al., 2014) and MAPK (Osinalde

Figure 1. Conditional Deletion of *Hhex* in NKp46-Expressing Cells Affects NK Cell Numbers but Not Maturation and Tumor Killing on a Per Cell Basis

(A) Bar graph depicting *Hhex* mRNA expression as measured by RNA sequencing of flow cytometrically sorted $CD3^{-}NK1.1^{+}NKp46^{+}$ splenic Imm ($CD11b^{-}KLRG1^{-}$), M1 ($CD11b^{+}KLRG1^{-}$), and M2 ($CD11b^{+}KLRG1^{+}$) NK cells.

(B) Representative western blot validating appreciable loss of HHEX in $CD3^{-}NK1.1^{+}NKp46^{+}$ splenic $Hhex^{\Delta/\Delta}$ NK cells. The housekeeping gene β-actin was used as loading control.

(C) Representative FACS plots demonstrating the identification of $NK1.1^{+}NKp46^{+}$ splenic NK cells after gating on viable $CD45^{+}CD3^{-}$ cells. Enumeration of absolute $CD3^{-}NK1.1^{+}NKp46^{+}$ NK cell numbers and their relative frequencies among $CD45^{+}$ cells in the spleens of *Cre* control and $Hhex^{\Delta/\Delta}$ mice.

(D) Flow cytometric analysis of NK cell maturation on the basis of CD11b and CD27 expression on NK cells (identified as in C) in the spleens and bone marrows of *Cre* control and $Hhex^{\Delta/\Delta}$ mice. Bar graphs indicate the absolute numbers of DN, Imm, M1, and M2 NK cells and their relative frequencies within the NK compartment.

(E) Flow cytometric analysis of activating receptor expression on NK cells ($CD3^{-}NK1.1^{+}NKp46^{+}CD49a^{-}CD49b^{+}$) from *Cre* control and $Hhex^{\Delta/\Delta}$ mice. Bar graphs depict the frequencies of *Cre* control and $Hhex^{\Delta/\Delta}$ NK cells that express the activating receptors Ly49D and Ly49H.

(F) Flow cytometric expression of NKG2D and DNAM-1 on *Cre* control and $Hhex^{\Delta/\Delta}$ NK cells ($CD3^{-}NK1.1^{+}NKp46^{+}CD49a^{-}CD49b^{+}$). Bar graphs depict the MFI of NKG2D and DNAM-1 staining among *Cre* control and $Hhex^{\Delta/\Delta}$ NK cells, as well as the proportion of *Cre* control and $Hhex^{\Delta/\Delta}$ NK cells that express DNAM-1.

(G) Frequencies of degranulating ($CD107a^{+}$) splenic $NK1.1^{+}NKp46^{+}CD49b^{+}Eomes^{+}$ NK cells after *ex vivo* stimulation with PMA and ionomycin, IL-12, and IL-18 or plate-bound antibodies against Ly49D, Ly49H, DNAM-1, NKG2D, and NKp46. As controls, cells were also incubated in wells that were not coated with antibodies.

(H) Percentage specific lysis of calcein-labeled B16F10 melanomas by expanded $Hhex^{\Delta/\Delta}$ NK cells (flow cytometrically sorted on viable $CD45^{+}CD3^{-}NK1.1^{+}NKp46^{+}CD49b^{+}$) at the E:T ratios indicated.

Results shown are from one experiment of at least three mice per genotype (A), one representative experiment of at least three mice per genotype (B–F), pooled from two experiments of at least three mice per genotype (G), and technical triplicates from one of three independent experiments (H). All bar graphs represent mean ± SD; each dot represents an individual mouse, except for graph depicting calcein release (H). Unpaired t tests; actual p values indicated. See also Figure S1.

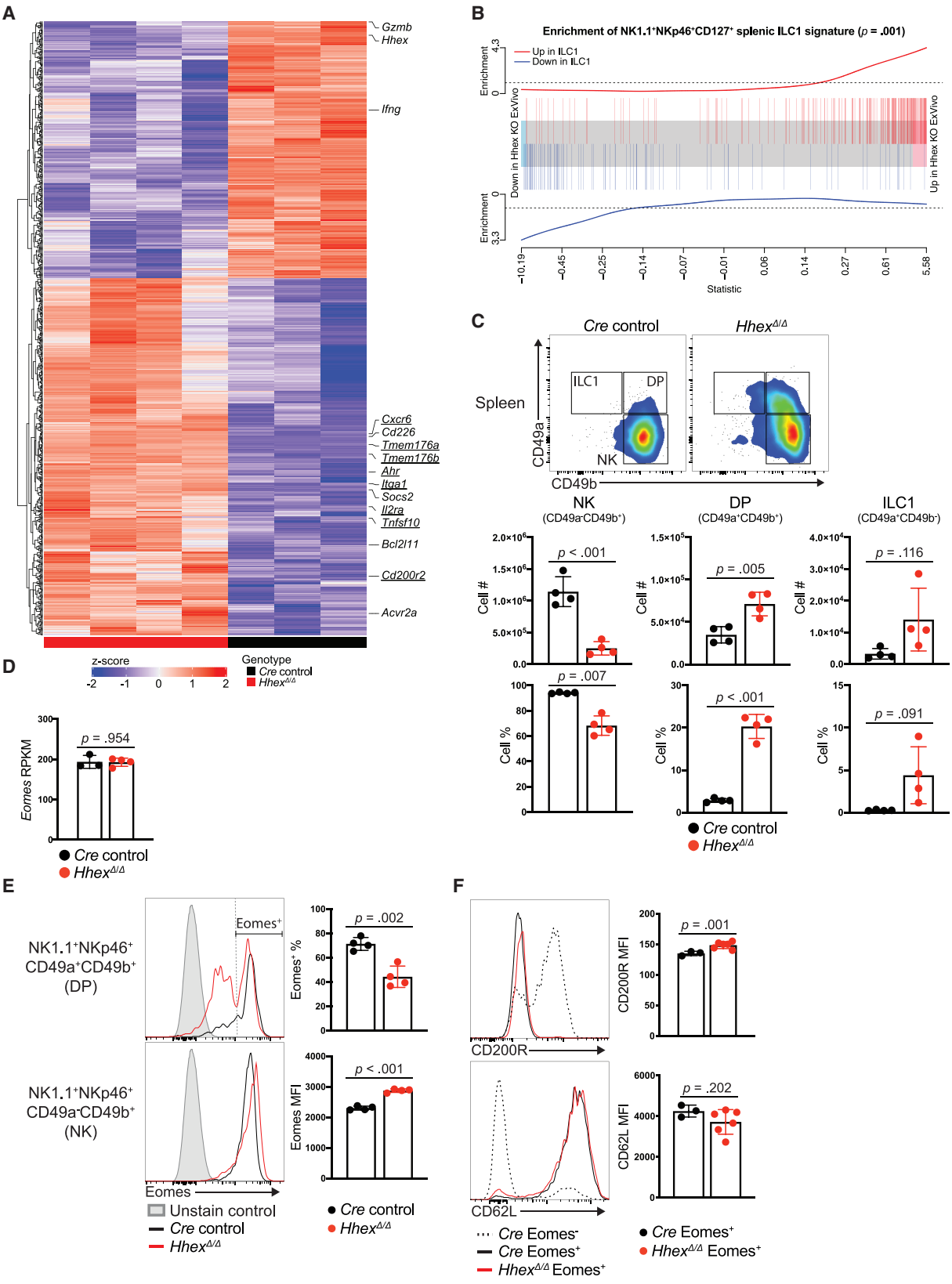

(legend on next page)

et al., 2015; Huntington et al., 2007a; Mishra et al., 2014) pathways, remain to be interrogated. Altogether, the data presented indicate that the loss of *Hhex* leads to NK cell hyper-proliferation that is not driven by aberrant IL-15 signaling via STAT5.

Aberrant Expression of Pro-survival and Pro-apoptotic Factors in the Absence of *Hhex* Cells Results in Impaired NK Cell Survival

Hhex$^{\Delta/\Delta}$ NK cells showed reduced accumulation despite a clear proliferative advantage *in vitro*, alluding to a defect in survival. This was evident with *Hhex*$^{\Delta/\Delta}$ NK cells that were cultured in 5 ng/mL rhIL-15, which supports NK cell survival rather than proliferation (Delconte et al., 2016a; Viant et al., 2017). Similarly, the loss of *Hhex* has previously been associated with increased apoptosis among immature B cell populations (Jackson et al., 2015). Although flow cytometric detection of activated caspase-3/7, which indicates irrevocable commitment to cell death (Nicholson et al., 1995; Slee et al., 1999), did not reveal significant differences in the frequencies of apoptotic NK cells *ex vivo* (Figure S3), this may be explained by avid clearance of apoptotic NK cells via phagocytic pathways (Carbonari et al., 1995; Gordon and Plüddemann, 2018).

Given that NK cell survival is determined by interactions between the key mediator of NK cell apoptosis BIM and anti-apoptotic factors such as BCL2 and MCL1 (Huntington et al., 2007a; Viant et al., 2017; Sathe et al., 2014), the expression of these apoptotic and survival factors in *Hhex*$^{\Delta/\Delta}$ NK cells was determined using flow cytometry (Figure 3F). *Hhex*$^{\Delta/\Delta}$ NK cells expressed significantly higher levels of BIM than *Cre* control NK cells, supporting increased apoptotic signaling in *Hhex*$^{\Delta/\Delta}$ NK cells. Differences in MCL1 expression between *Cre* control and *Hhex*$^{\Delta/\Delta}$ NK cells, though statistically significant, were mild and deemed unlikely to affect *Hhex*$^{\Delta/\Delta}$ NK cell survival. Unexpectedly, BCL2 expression was also significantly increased, potentially to compensate for increased BIM expression. BCL2, a pro-survival protein that is induced by IL-15, has been shown to bind and antagonize BIM in NK cells (Huntington et al., 2007a). To determine if further augmenting BCL2 levels could also rescue *Hhex*-deficient NK cells from increased BIM-mediated apoptosis *in vivo*, mixed bone marrow chimeras were generated (Figure 3G). Consistent with published findings (Ogilvy et al., 1999), *Bcl2* transgene expression resulted in the over-representation of *Hhex*-sufficient hematopoietic cells as well as NK cells (Figure 3H). This advantage was retained when *Hhex* was systemically inactivated by Cre recombinase expressed under control of the *Mx1* promoter (Kühn et al., 1995), providing further evidence for impaired cell survival, most likely due to overwhelming BIM levels, as the primary reason for NK cell loss in *Hhex*$^{\Delta/\Delta}$ mice.

Hhex Promotes NK Cell Survival by Direct Repression of *Bcl2l11* Expression

To assess the extent to which increased BIM levels influenced NK cell numbers in *Hhex*$^{\Delta/\Delta}$ mice, *Bcl2l11* (gene encoding BIM) and *Hhex* were concomitantly inactivated in NKp46-expressing cells. Remarkably, the proportion and total numbers of NK cells in all hematopoietic tissues of *Hhex*$^{\Delta/\Delta}$*Bim*$^{\Delta/\Delta}$ mice were comparable with *Cre* control mice (Figure 4A), confirming BIM-mediated apoptosis as the key driver of NK cell lymphopenia in *Hhex*$^{\Delta/\Delta}$ mice. In order to investigate if HHEX directly inhibits BIM expression by binding to the *Bcl2l11* gene, we performed cleavage under targets and release using nuclease (CUT&RUN [CnR]) sequencing, a more sensitive technique that is based on the main principles of chromatin immunoprecipitation (ChIP) sequencing (Skene and Henikoff, 2017). GREAT analysis of peaks called by MACS2 revealed 1,554 genes in the proximity (within 0.1 kB) of HHEX binding sites. Comparing these genes with those that were differentially expressed in the absence of HHEX (RNA-seq; Figure 2A), we identified 55 common genes (Figure 4B). One of the common genes was *Bcl2l11*, and direct binding of HHEX to its promoter region was observed (Figure 4B). These data confirm a direct role for HHEX in repressing *Bcl2l11*-mediated NK cell apoptosis and a mechanism behind the essential role of HHEX in normal NK cell lymphopoiesis *in vivo*. The hyper-proliferative phenotype of *Hhex*$^{\Delta/\Delta}$ NK cells was also reversed with the additional deletion of *Bcl2l11*, as indicated by similar frequencies of Ki-67^{+} NK cells in the spleens of *Hhex*$^{\Delta/\Delta}$*Bim*$^{\Delta/\Delta}$ mice and *Cre* control mice (Figure 4C). Counter-intuitively, these results also suggest that the hyper-proliferation *Hhex*$^{\Delta/\Delta}$ NK was driven largely by intrinsically high BIM levels and to some degree a homeostatic response to reduced NK cell numbers, rather than the direct regulation of NK cell proliferation

Figure 2. *Hhex* Inactivation Results in Enrichment of ILC1 Signature Genes and Augments Frequencies of Eomes^{-}CD49a^{+}CD49b^{+} (DP) Cells

(A and B) RNA-seq analysis of differentially expressed genes (DEGs) between CD45^{+}CD3^{-}CD19^{-}NK1.1^{+}NKp46^{+}CD49b^{+} splenic NK cells from *Cre* control and *Hhex*$^{\Delta/\Delta}$ mice. (A) Heatmap of all DEGs (FDR < 0.05) between biological replicates of *Cre* control and *Hhex*$^{\Delta/\Delta}$ NK cells. The genes annotated includes genes of interest and ILC1 signature genes (underlined). Color key shows *Z* score values for the heatmap. (B) Barcode plot depicting enrichment of a previously described ILC1 gene signature in *Hhex*$^{\Delta/\Delta}$ NK cells. Genes from the dataset were ranked by moderated t statistics; upregulated genes shaded in pink and downregulated genes shaded in blue. Signature genes are indicated on the plot as vertical lines. The position of each individual gene along the plot reflects the significance of differential expression, and the direction of differential expression is colored red for upregulation or blue for downregulation.

(C) Representative flow cytometry plots demonstrating the identification of NK (CD49a^{-}CD49b^{+}), DP (CD49a^{+}CD49b^{+}), and ILC1 (CD49a^{+}CD49b^{-}) after gating on viable CD45^{+}CD3^{-}NK1.1^{+}NKp46^{+} cells. Enumeration of absolute NK, DP, and ILC1 numbers and their relative frequencies within the group 1 ILC compartment (viable CD45^{+}CD3^{-}NK1.1^{+}NKp46^{+}) in spleens of *Cre* control and *Hhex*$^{\Delta/\Delta}$ mice.

(D) Bar graph depicting transcript abundance of *Eomes* in NK1.1^{+}NKp46^{+}CD49b^{+} cells as determined by RNA-seq.

(E) Flow cytometric analysis of Eomes expression among splenic DP and NK cells of *Cre* control and *Hhex*$^{\Delta/\Delta}$ mice. Bar graphs depict Eomes expression with respect to the frequency of Eomes-expressing (Eomes^{+}) DPs or the median fluorescence intensity (MFI) of Eomes staining among NK cells.

(F) Representative histograms demonstrating CD200R and CD62L expression on Eomes^{+} liver NK cells of *Cre* control and *Hhex*$^{\Delta/\Delta}$ mice in relation to Eomes^{-} liver ILC1 of *Cre* control mice. Bar graphs depict quantitation of CD200R and CD62L expression on Eomes^{+} NK cells from the livers of *Cre* control and *Hhex*$^{\Delta/\Delta}$ mice. Results shown are from one experiment of at least three mice per genotype (A and B) and one experiment of at least three mice per genotype (C–F). All bar graphs represent mean ± SD; each dot represents an individual mouse. Unpaired t tests; actual p values indicated. See also Figure S2.

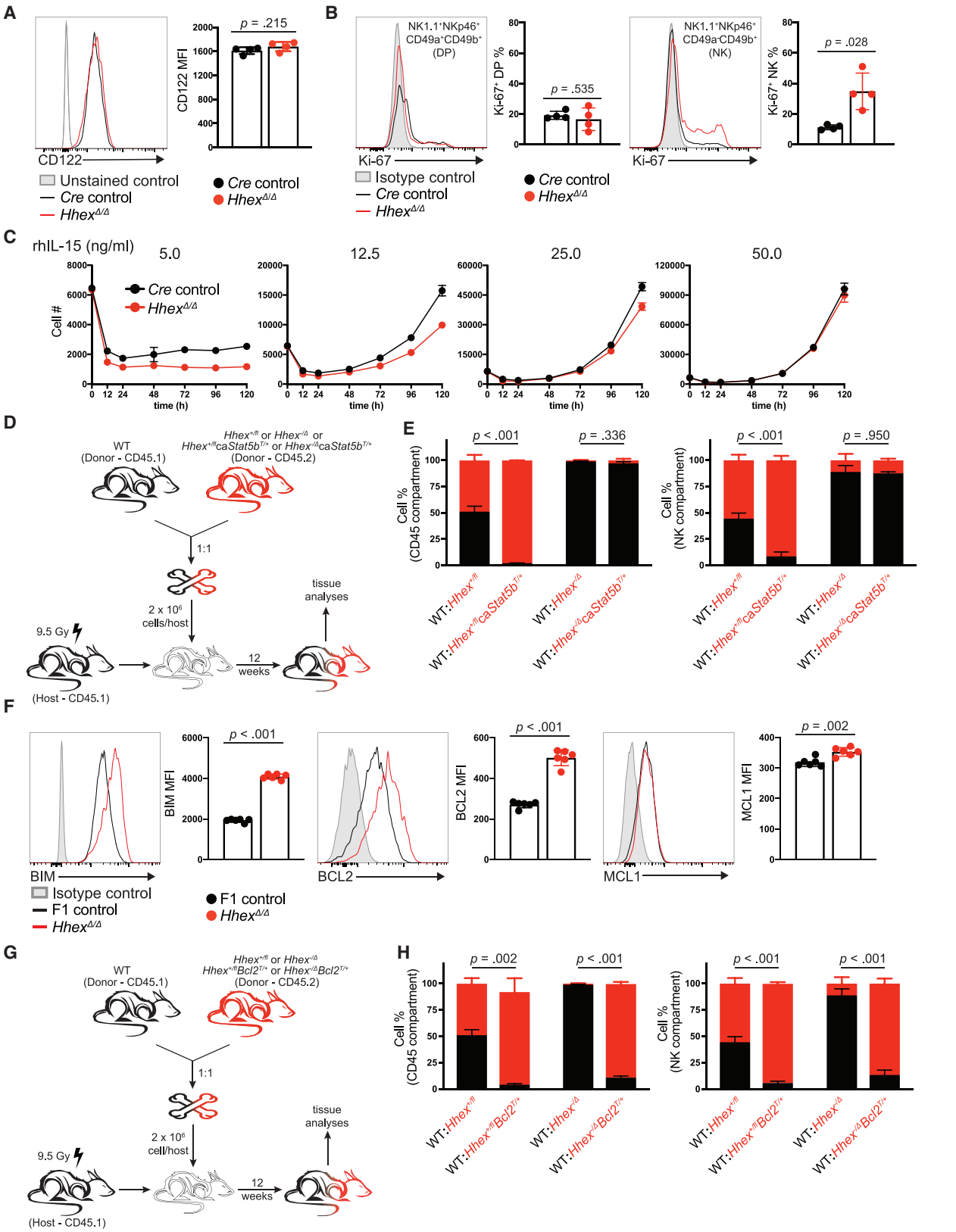

(legend on next page)

by *Hhex*. Taken together, the data presented show that *Hhex* regulates NK cell survival and ultimately NK cell numbers, by directly repressing *Bcl2l11* expression and subsequently BIM-mediated apoptosis.

Robust NK Cell Response to MCMV Infection in the Absence of *Hhex*

Given that NK cell frequency and turnover was restored in $Hhex^{\Delta/\Delta}Bim^{\Delta/\Delta}$ mice, we examined the *in vivo* impact of *Hhex* deficiency on NK cell function by challenging these mice with murine cytomegalovirus (MCMV). During the acute phase MCMV infection, NK cells that express Ly49H are able to recognize the m157 MCMV glycoprotein and undergo rapid expansion, driven by IL-12 and IL-18 to mediate rapid immunity via IFN-γ production (Arase et al., 2002; Brown et al., 2001; Dokun et al., 2001; Smith et al., 2002). We compared total NK and Ly49H$^+$ NK cell numbers between naive and infected $Hhex^{\Delta/\Delta}$, $Hhex^{\Delta/\Delta}Bim^{\Delta/\Delta}$, and *Cre* control mice. Although $Hhex^{\Delta/\Delta}$ mice possessed far fewer total and Ly49H$^+$ NK cells than *Cre* control mice by 7 days post-infection (i.e., end of expansion phase), NK cells of infected $Hhex^{\Delta/\Delta}$ mice trended toward higher fold expansions, which was statistically significant for the Ly49H$^+$ subset (Figure 4D). The fold expansion of $Hhex^{\Delta/\Delta}Bim^{\Delta/\Delta}$ remained similar to *Cre* control mice, which agrees with previous findings that *Bim* is at least dispensable for NK cell expansion during MCMV infection (Min-Oo et al., 2014) and reiterates the requirement for *Hhex* during NK cell proliferation *in vivo*. Unexpectedly, viral titers in the spleens, livers, and lungs of $Hhex^{\Delta/\Delta}$ mice were not significantly higher than those of *Cre* control or $Hhex^{\Delta/\Delta}Bim^{\Delta/\Delta}$ mice (Figure 4E), which suggests that only a relatively small number of functionally competent NK cells are required to mediate a protective response against MCMV infections.

In summary, we have shown that the survival and consequently homeostatic maintenance of lineage-committed NK cells is intrinsically dependent on *Hhex*. The pro-survival role of *Hhex* is maintained throughout NK cell maturation, as *Hhex* deletion does not result in the selective loss of a particular maturational subset. NK cell development, function, and survival are classically thought to be critically dependent on IL-15 (Kennedy et al., 2000; Cooper et al., 2002; Huntington et al., 2007a). Furthermore, IL-15 signaling has been shown to induce BCL2 that antagonizes BIM in NK cells (Huntington et al., 2007a). As such, it was surprising to find that enforced IL-15 signaling by constitutive activation of STAT5 did not augment BCL2 to levels that would overcome the intrinsically high levels of BIM levels in $Hhex^{\Delta/\Delta}$ NK cells and promote NK cell survival, suggesting that IL-15-independent pathways are involved. Although IL-15-independent NK cell responses have been described in MCMV-infected mice (Sun et al., 2009) and vaccinia-infected mice (Ohs et al., 2016), where NK cell proliferation is instead driven by IL-12, we have no evidence that IL-12 signaling or IFN-γ production in response to IL-12 is altered in $Hhex^{\Delta/\Delta}$ NK cells. Coincidentally, RNA-seq analysis revealed that expression of *Il2ra* (gene encoding IL-2Rα or CD25) was significantly increased in *Hhex*-deficient NK cells, suggesting increased sensitivity to IL-2. As such, future studies on responses to IL-2 may shed further light on the present findings and reveal subtle differences between the receptor subunits and signaling pathways that are co-utilized by IL-2 and IL-15 (Osinalde et al., 2015).

Hhex has been previously been implicated in the regulation of HSC self-renewal and early lymphoid progenitor development via active repression of the cell cycle inhibitor *Cdkn2a* (Jackson et al., 2015, 2017; Goodings et al., 2015). In contrast, *Cdkn2a* expression was not upregulated in *Hhex*-deficient NK cells, which instead showed increased DNA replication and expression of cell cycle genes such as *Mki67*, *Cdk2*, *Cdk6*, and *E2f3* (Baychelier and Vieillard, 2013; Jung et al., 2012). Thus, the mechanism by which *Hhex* controls cell cycle in NK cells is likely a distinct from HSC and other lymphocytes.

Bioinformatic analyses have revealed a significant enrichment of ILC1 signature genes in CD3$^-$NK1.1$^+$NKp46$^+$CD49b$^+$ cells,

Figure 3. Increased IL-15-Independent NK Cell Turnover in the Absence of *Hhex*

(A) Flow cytometric assessment of IL-15Rβ (CD122) subunit expression (MFI) on splenic NK cells (CD3$^-$NK1.1$^+$NKp46$^+$CD49a$^-$CD49b$^+$) from *Cre* control and $Hhex^{\Delta/\Delta}$ mice.

(B) Flow cytometric analysis of DP and NK cell turnover in *Cre* control and $Hhex^{\Delta/\Delta}$ mice by Ki-67 expression. Bar graphs depict the frequencies of Ki-67 expressing splenic DP and NK cells from *Cre* control or $Hhex^{\Delta/\Delta}$ mice expression as determined by intracellular antibody staining. A matching isotype control was used to discern non-specific binding.

(C) CD3$^-$CD19$^-$NK1.1$^+$NKp46$^+$CD49b$^+$ *Cre* control and $Hhex^{\Delta/\Delta}$ NK cells were CTV-labeled and cultured in 5, 12.5, 25, and 50 ng/mL IL-15. Viable cell numbers were enumerated after the indicated time in culture.

(D and E) Assessing rescue of $Hhex^{\Delta/\Delta}$ NK cells by constitutive activation of *Stat5b* (ca*Stat5b*). (D) Schematic of 50:50 bone marrow chimeric setup. Unfractionated bone marrow from CD45.1$^+$ WT control donors and either CD45.2$^+$ $Hhex^{+/fl}$, $Hhex^{-/\Delta}$, $Hhex^{+/fl}$ca$Stat5b^{T/+}$, or $Hhex^{-/\Delta}$ca$Stat5b^{T/+}$ experimental donors were transplanted into lethally irradiated CD45.1$^+$ recipients. (E) Hematopoietic and NK cell reconstitution was assessed 12 weeks post-transplantation. Bar graphs represent frequencies or ratios of WT and either $Hhex^{+/fl}$, $Hhex^{-/\Delta}$, $Hhex^{+/fl}$ca$Stat5b^{T/+}$, or $Hhex^{-/\Delta}$ca$Stat5b^{T/+}$ hematopoietic (CD45$^+$) and NK cells retrieved from the spleens of mixed bone marrow chimeras.

(F) Flow cytometric determination of BIM, BCL2, and MCL1 expression in F1 control or $Hhex^{\Delta/\Delta}$ NK cells (CD3$^-$NK1.1$^+$NKp46$^+$Eomes$^+$) retrieved from the spleen and bone marrow of F1:$Hhex^{\Delta/\Delta}$ mixed bone marrow chimeras.

(G and H) Assessing rescue of *Hhex*-deficient NK cells by *Bcl2* overexpression. (G) Schematic of 50:50 bone marrow chimeric setup. Unfractionated bone marrow from CD45.1$^+$ WT control donors and either CD45.2$^+$ $Hhex^{+/fl}$, $Hhex^{-/\Delta}$, $Hhex^{+/fl}Bcl2^{T/+}$, or $Hhex^{-/\Delta}Bcl2^{T/+}$ experimental donors were transplanted into lethally irradiated CD45.1$^+$ recipients.

(H) Hematopoietic and NK cell reconstitution was assessed 12 weeks post-transplantation. Bar graphs represent frequencies or ratios of WT and either $Hhex^{+/fl}$, $Hhex^{-/\Delta}$, $Hhex^{+/fl}Bcl2^{T/+}$, or $Hhex^{-/\Delta}Bcl2^{T/+}$ hematopoietic (CD45$^+$) and NK cells retrieved from the spleens of mixed bone marrow chimeras.

Results shown are from one representative experiment of at least three mice per genotype (A and B), technical triplicates from one of two independent experiments (C), three pooled experiments (D, E, G, and H) and donor pairs of F1 control and $Hhex^{\Delta/\Delta}$ mice reconstituting six recipients (F). All bar and line graphs represent mean ± SD; each dot on bar graphs represents an individual mouse, except for graph depicting *in vitro* expansion of CTV labeled NK cells (C). Unpaired t tests; actual p values indicated. See also Figure S3.

CellPress
OPEN ACCESS

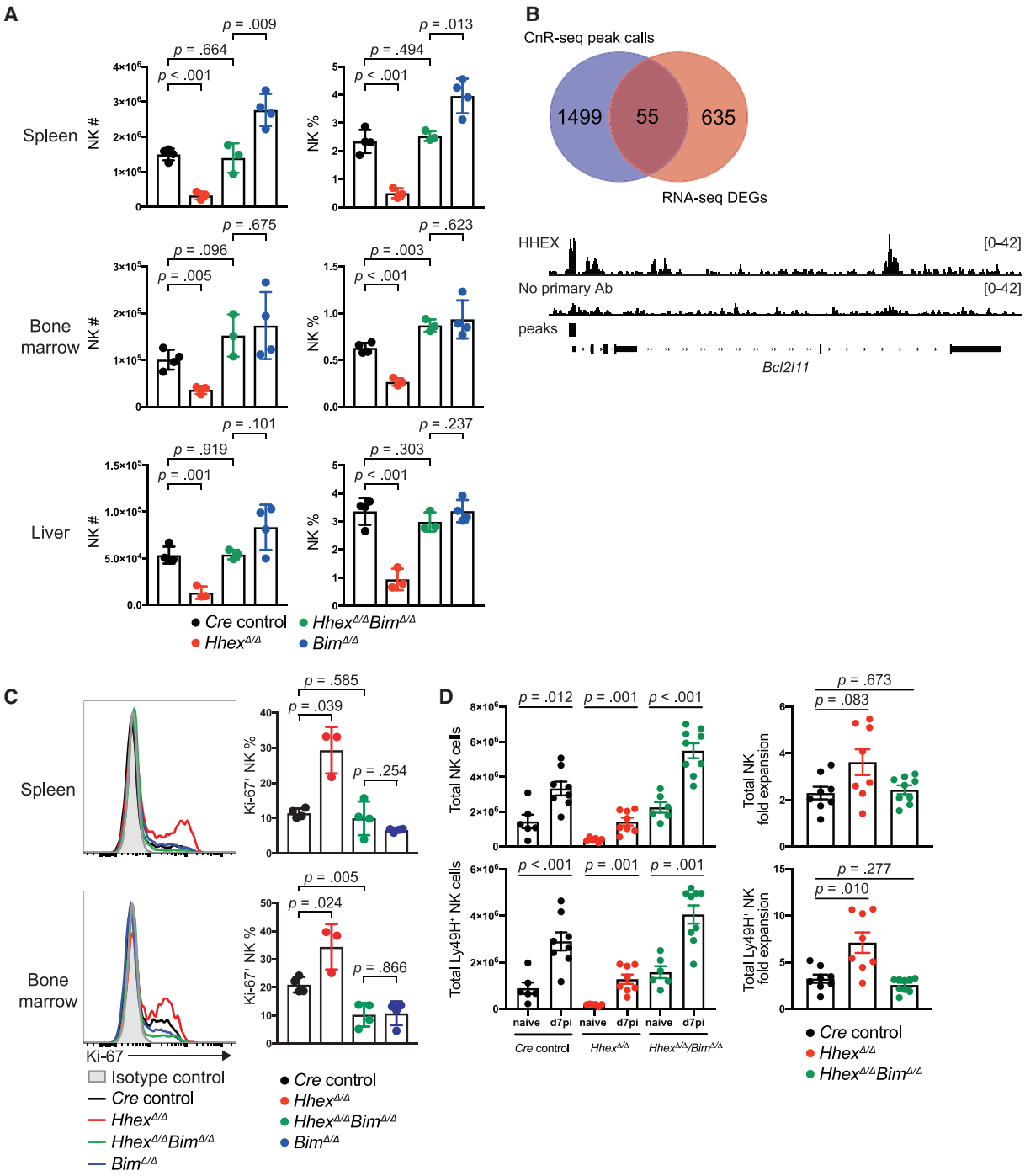

(legend on next page)

traditionally defined as NK cells, in the absence of *Hhex*. This clearly highlights the limitations of the markers that are typically used to identify NK cells and distinguish them from ILC1s, which is further compounded by phenotypic and functional heterogeneity among group 1 ILCs (O'Sullivan, 2019; Gao et al., 2017; Rautela et al., 2019). That said, *Hhex* clearly has a dominant effect on the frequency of NK cell numbers compared with other ILC1s despite similar expression of *Hhex*, and this may be due in part to the intrinsically low cell cycle and inert nature of ILC1 compared with NK cells. In conclusion, this study presents the first evidence that *Hhex* functions to maintain NK cell homeostasis by repressing BIM-mediated NK cell apoptosis.

STAR★METHODS

Detailed methods are provided in the online version of this paper and include the following:

- KEY RESOURCES TABLE
- RESOURCE AVAILABILITY
  - Lead Contact
  - Materials Availability
  - Data and Code Availability
- EXPERIMENTAL MODEL AND SUBJECT DETAILS
  - Mice
  - Cells
  - Viruses
- METHOD DETAILS
  - Bone marrow chimeras
  - Flow cytometry and cell sorting
  - NK cell stimulation and proliferation
  - Calcein release assay
  - Murine cytomegalovirus infection
  - EdU incorporation assay
  - SDS polyacrylamide gel electrophoresis and western blotting
  - RNA sequencing and data analysis
  - CUT&RUN
- QUANTIFICATION AND STATISTICAL ANALYSIS

SUPPLEMENTAL INFORMATION

Supplemental Information can be found online at https://doi.org/10.1016/j.celrep.2020.108285.

ACKNOWLEDGMENTS

We wish to thank C. Quillici, T. Camilleri, T. Kratina, E. Surgenor, F. Souza-Fonseca-Guimaraes, L. O'Reilly, and S. Wilcox for providing technical assistance and reagents. E. Vivier provided *Ncr1*^{iCre} mice, and M.J. Herold provided *Bim*$^{fl/fl}$ mice. We are grateful to WEHI Bioservices, monoclonal antibody facility, flow cytometry laboratory, and Clinical Translational Centre. W.G. is supported by a Melbourne International Research Scholarship. This work is supported by project grants from the National Health and Medical Research Council (NHMRC) of Australia (GNT1124784, GNT1066770, GNT1057852, GNT1124907, GNT1057812, GNT1049407, GNT1027472, and GNT1184615 to N.D.H.) and an NHMRC Investigator Fellowship (GNT1195296 to N.D.H.). N.D.H. is a recipient of a Melanoma Research Grant from the Harry J. Lloyd Charitable Trust, Melanoma Research Alliance Young Investigator Award, an Ian Potter Foundation equipment grant, the National Foundation for Medical Research and Innovation (NFMRI) John Dixon Hughes Medal, and a CLIP grant from Cancer Research Institute. S.L.N. is a NHMRC SPRF Fellow (GNT1155342). M.A.D.-E. is a NHMRC PRF Fellow (GNT1119298). J.R. was supported by a Victorian Cancer Agency grant (ECSG18020).

AUTHOR CONTRIBUTIONS

W.G., J.T.J., R.B.D., C.E.A., I.S.S., S.S., and J.R. designed and performed experiments. S.H.-Z. and S.S. provided bioinformatics analysis and input into interpretation of results. N.D.H., S.L.N., M.P.M., M.J.D., and M.A.D.-E. supervised experimental design and provided input into interpretation of results. M.P.M. provided *Hhex*$^{fl/fl}$ mice. W.G., S.L.N., and N.D.H. wrote the manuscript with editorial input from all authors.

DECLARATION OF INTERESTS

N.D.H. and J.R. are cofounders and shareholders in oNKo-Innate. The other authors declared no competing interests.

Received: December 11, 2019
Revised: August 17, 2020
Accepted: September 25, 2020
Published: October 20, 2020

REFERENCES

Adams, N.M., Lau, C.M., Fan, X., Rapp, M., Geary, C.D., Weizman, O.-E., Diaz-Salazar, C., and Sun, J.C. (2018). Transcription factor IRF8 orchestrates the adaptive natural killer cell response. Immunity *48*, 1172–1182.e6.

Ali, A.K., Nandagopal, N., and Lee, S.-H. (2015). IL-15–PI3K–AKT–mTOR: a critical pathway in the life journey of natural killer cells. Front. Immunol. *6*, 355.

Arase, H., Mocarski, E.S., Campbell, A.E., Hill, A.B., and Lanier, L.L. (2002). Direct recognition of cytomegalovirus by activating and inhibitory NK cell receptors. Science *296*, 1323–1326.

Figure 4. *Hhex* Promotes NK Cell Survival via Direct Repression of BIM

(A) Flow cytometric assessment of absolute NK cell (CD3$^-$NK1.1$^+$NKp46$^+$CD49a$^-$CD4b$^+$) numbers and their relative frequencies among CD45$^+$ cells in the indicated organs of *Cre* control, *Hhex*$^{\Delta/\Delta}$, *Hhex*$^{\Delta/\Delta}$*Bim*$^{\Delta/\Delta}$, and *Bim*$^{\Delta/\Delta}$ mice.

(B) HHEX CUT&RUN of nuclei isolated from C57BL/6 WT NK cells that were cultured in the presence of rhIL-15 for 5 days. Venn diagram of GREAT analysis of MACS2-called peaks and DEGs from RNA-seq and the overlapping genes. Tracks show HHEX binding at the *Bcl2l11* gene including MACS2-called peak. No primary Ab track acts as an input control.

(C) Ki-67 expression in NK cells (CD3$^-$NK1.1$^+$NKp46$^+$CD49a$^-$CD4b$^+$) from the spleen and bone marrow of *Cre* control, *Hhex*$^{\Delta/\Delta}$, *Hhex*$^{\Delta/\Delta}$*Bim*$^{\Delta/\Delta}$, and *Bim*$^{\Delta/\Delta}$ mice.

(D and E) Viral responses in the absence of *Hhex* was assessed by infecting *Cre* control and *Hhex*$^{\Delta/\Delta}$ mice with MCMV. (D) Absolute numbers and corresponding fold expansion of total and Ly49H$^+$ NK cells (CD3$^-$NK1.1$^+$NKp46$^+$) in the spleens of naive and MCMV-infected (7 days post-infection) mice. (E) Viral titers in the spleens, livers, and lungs of MCMV-infected mice as determined by plaque assay. Dotted line indicates the limit of detection of the assay.

Results shown are from one experiment of at least three mice per genotype (A and C), one experiment of one WT mouse (B), and two pooled experiments (D and E). All bar graphs represent mean ± SD; each dot represents an individual mouse. Unpaired t tests applied in (A) and (C); Mann-Whitney test applied in (D) and (E); actual p values indicated.

Assmann, N., O'Brien, K.L., Donnelly, R.P., Dyck, L., Zaiatz-Bittencourt, V., Loftus, R.M., Heinrich, P., Oefner, P.J., Lynch, L., Gardiner, C.M., et al. (2017). Srebp-controlled glucose metabolism is essential for NK cell functional responses. Nat. Immunol. *18*, 1197–1206.

Baychelier, F., and Vieillard, V. (2013). The modulation of the cell-cycle: a sentinel to alert the NK cells of dangers. Front. Immunol. *4*, 325.

Bedford, F.K., Ashworth, A., Enver, T., and Wiedemann, L.M. (1993). HEX: a novel homeobox gene expressed during haematopoiesis and conserved between mouse and human. Nucleic Acids Res. *21*, 1245–1249.

Bogue, C.W., Ganea, G.R., Sturm, E., Ianucci, R., and Jacobs, H.C. (2000). Hex expression suggests a role in the development and function of organs derived from foregut endoderm. Dev. Dyn. *219*, 84–89.

Bogue, C.W., Zhang, P.-X., McGrath, J., Jacobs, H.C., and Fuleihan, R.L. (2003). Impaired B cell development and function in mice with a targeted disruption of the homeobox gene Hex. Proc. Natl. Acad. Sci. U S A *100*, 556–561.

Brown, M.G., Dokun, A.O., Heusel, J.W., Smith, H.R., Beckman, D.L., Blattenberger, E.A., Dubbelde, C.E., Stone, L.R., Scalzo, A.A., and Yokoyama, W.M. (2001). Vital involvement of a natural killer cell activation receptor in resistance to viral infection. Science *292*, 934–937.

Burchill, M.A., Goetz, C.A., Prlic, M., O'Neil, J.J., Harmon, I.R., Bensinger, S.J., Turka, L.A., Brennan, P., Jameson, S.C., and Farrar, M.A. (2003). Distinct effects of STAT5 activation on CD4+ and CD8+ T cell homeostasis: development of CD4+CD25+ regulatory T cells versus CD8+ memory T cells. J. Immunol. *171*, 5853–5864.

Carbonari, M., Cibati, M., and Fiorilli, M. (1995). Measurement of apoptotic cells in peripheral blood. Cytometry *22*, 161–167.

Carson, W.E., Giri, J.G., Lindemann, M.J., Linett, M.L., Ahdieh, M., Paxton, R., Anderson, D., Eisenmann, J., Grabstein, K., and Caligiuri, M.A. (1994). Interleukin (IL) 15 is a novel cytokine that activates human natural killer cells via components of the IL-2 receptor. J. Exp. Med. *180*, 1395–1403.

Castro, W., Chelbi, S.T., Niogret, C., Ramon-Barros, C., Welten, S.P.M., Osterheld, K., Wang, H., Rota, G., Morgado, L., Vivier, E., et al. (2018). The transcription factor Rfx7 limits metabolism of NK cells and promotes their maintenance and immunity. Nat. Immunol. *19*, 809–820.

Chiossone, L., Chaix, J., Fuseri, N., Roth, C., Vivier, E., and Walzer, T. (2009). Maturation of mouse NK cells is a 4-stage developmental program. Blood *113*, 5488–5496.

Cooper, M.A., Bush, J.E., Fehniger, T.A., VanDeusen, J.B., Waite, R.E., Liu, Y., Aguila, H.L., and Caligiuri, M.A. (2002). In vivo evidence for a dependence on interleukin 15 for survival of natural killer cells. Blood *100*, 3633–3638.

Crompton, M.R., Bartlett, T.J., MacGregor, A.D., Manfioletti, G., Buratti, E., Giancotti, V., and Goodwin, G.H. (1992). Identification of a novel vertebrate homeobox gene expressed in haematopoietic cells. Nucleic Acids Res. *20*, 5661–5667.

de Graaf, C.A., Choi, J., Baldwin, T.M., Bolden, J.E., Fairfax, K.A., Robinson, A.J., Biben, C., Morgan, C., Ramsay, K., Ng, A.P., et al. (2016). Haemopedia: an expression atlas of murine hematopoietic cells. Stem Cell Reports *7*, 571–582.

Delconte, R.B., Kolesnik, T.B., Dagley, L.F., Rautela, J., Shi, W., Putz, E.M., Stannard, K., Zhang, J.-G., Teh, C., Firth, M., et al. (2016a). CIS is a potent checkpoint in NK cell-mediated tumor immunity. Nat. Immunol. *17*, 816–824.

Delconte, R.B., Shi, W., Sathe, P., Ushiki, T., Seillet, C., Minnich, M., Kolesnik, T.B., Rankin, L.C., Mielke, L.A., Zhang, J.-G., et al. (2016b). The helix-loop-helix protein ID2 governs NK cell fate by tuning their sensitivity to interleukin-15. Immunity *44*, 103–115.

Dobin, A., Davis, C.A., Schlesinger, F., Drenkow, J., Zaleski, C., Jha, S., Batut, P., Chaisson, M., and Gingeras, T.R. (2013). STAR: ultrafast universal RNA-seq aligner. Bioinformatics *29*, 15–21.

Dokun, A.O., Kim, S., Smith, H.R.C., Kang, H.-S.P., Chu, D.T., and Yokoyama, W.M. (2001). Specific and nonspecific NK cell activation during virus infection. Nat. Immunol. *2*, 951–956.

Donnelly, R.P., Loftus, R.M., Keating, S.E., Liou, K.T., Biron, C.A., Gardiner, C.M., and Finlay, D.K. (2014). mTORC1-dependent metabolic reprogramming is a prerequisite for NK cell effector function. J. Immunol. *193*, 4477–4484.

Fehniger, T.A., Suzuki, K., Ponnappan, A., VanDeusen, J.B., Cooper, M.A., Florea, S.M., Freud, A.G., Robinson, M.L., Durbin, J., and Caligiuri, M.A. (2001). Fatal leukemia in interleukin 15 transgenic mice follows early expansions in natural killer and memory phenotype CD8+ T cells. J. Exp. Med. *193*, 219–231.

Gao, Y., Souza-Fonseca-Guimaraes, F., Bald, T., Ng, S.S., Young, A., Ngiow, S.F., Rautela, J., Straube, J., Waddell, N., Blake, S.J., et al. (2017). Tumor immunoevasion by the conversion of effector NK cells into type 1 innate lymphoid cells. Nat. Immunol. *18*, 1004–1015.

Gehring, W.J. (1987). Homeo boxes in the study of development. Science *236*, 1245–1252.

Ghosh, B., Jacobs, H.C., Wiedemann, L.M., Brown, A., Bedford, F.K., Nimmakayalu, M.A., Ward, D.C., and Bogue, C.W. (1999). Genomic structure, cDNA mapping, and chromosomal localization of the mouse homeobox gene, Hex. Mamm. Genome *10*, 1023–1025.

Goh, W., and Huntington, N.D. (2017). Regulation of murine natural killer cell development. Front. Immunol. *8*, 130.

Goodings, C., Smith, E., Mathias, E., Elliott, N., Cleveland, S.M., Tripathi, R.M., Layer, J.H., Chen, X., Guo, Y., Shyr, Y., et al. (2015). Hhex is required at multiple stages of adult hematopoietic stem and progenitor cell differentiation. Stem Cells *33*, 2628–2641.

Gordon, S., and Plüddemann, A. (2018). Macrophage clearance of apoptotic cells: a critical assessment. Front. Immunol. *9*, 127.

Guiral, M., Bess, K., Goodwin, G., and Jayaraman, P.S. (2001). PRH represses transcription in hematopoietic cells by at least two independent mechanisms. J. Biol. Chem. *276*, 2961–2970.

Guo, Y., Chan, R., Ramsey, H., Li, W., Xie, X., Shelley, W.C., Martinez-Barbera, J.P., Bort, B., Zaret, K., Yoder, M., and Hromas, R. (2003). The homeoprotein Hex is required for hemangioblast differentiation. Blood *102*, 2428–2435.

Hallaq, H., Pinter, E., Enciso, J., McGrath, J., Zeiss, C., Brueckner, M., Madri, J., Jacobs, H.C., Wilson, C.M., Vasavada, H., et al. (2004). A null mutation of Hhex results in abnormal cardiac development, defective vasculogenesis and elevated Vegfa levels. Development *131*, 5197–5209.

Hayakawa, Y., and Smyth, M.J. (2006). CD27 dissects mature NK cells into two subsets with distinct responsiveness and migratory capacity. J. Immunol. *176*, 1517–1524.

Heng, T.S.P., and Painter, M.W.; Immunological Genome Project Consortium (2008). The Immunological Genome Project: networks of gene expression in immune cells. Nat. Immunol. *9*, 1091–1094.

Hennessy, R.J., Pham, K., Delconte, R., Rautela, J., Hodgkin, P.D., and Huntington, N.D. (2019). Quantifying NK cell growth and survival changes in response to cytokines and regulatory checkpoint blockade helps identify optimal culture and expansion conditions. J. Leukoc. Biol. *105*, 1341–1354.

Herold, M.J., Stuchbery, R., Mérino, D., Willson, T., Strasser, A., Hildeman, D., and Bouillet, P. (2014). Impact of conditional deletion of the pro-apoptotic BCL-2 family member BIM in mice. Cell Death Dis. *5*, e1446.

Hromas, R., Radich, J., and Collins, S. (1993). PCR cloning of an orphan homeobox gene (PRH) preferentially expressed in myeloid and liver cells. Biochem. Biophys. Res. Commun. *195*, 976–983.

Hunter, M.P., Wilson, C.M., Jiang, X., Cong, R., Vasavada, H., Kaestner, K.H., and Bogue, C.W. (2007). The homeobox gene Hhex is essential for proper hepatoblast differentiation and bile duct morphogenesis. Dev. Biol. *308*, 355–367.

Huntington, N.D., Puthalakath, H., Gunn, P., Naik, E., Michalak, E.M., Smyth, M.J., Tabarias, H., Degli-Esposti, M.A., Dewson, G., Willis, S.N., et al. (2007a). Interleukin 15-mediated survival of natural killer cells is determined by interactions among Bim, Noxa and Mcl-1. Nat. Immunol. *8*, 856–863.

Huntington, N.D., Tabarias, H., Fairfax, K., Brady, J., Hayakawa, Y., Degli-Esposti, M.A., Smyth, M.J., Tarlinton, D.M., and Nutt, S.L. (2007b). NK cell maturation and peripheral homeostasis is associated with KLRG1 up-regulation. J. Immunol. *178*, 4764–4770.

Huntington, N.D., Legrand, N., Alves, N.L., Jaron, B., Weijer, K., Plet, A., Corcuff, E., Mortier, E., Jacques, Y., Spits, H., and Di Santo, J.P. (2009). IL-15 trans-presentation promotes human NK cell development and differentiation in vivo. J. Exp. Med. *206*, 25–34.

Huntington, N.D., Cursons, J., and Rautela, J. (2020). The cancer-natural killer cell immunity cycle. Nat. Rev. Cancer *20*, 437–454.

Jackson, J.T., Nasa, C., Shi, W., Huntington, N.D., Bogue, C.W., Alexander, W.S., and McCormack, M.P. (2015). A crucial role for the homeodomain transcription factor Hhex in lymphopoiesis. Blood *125*, 803–814.

Jackson, J.T., Shields, B.J., Shi, W., Di Rago, L., Metcalf, D., Nicola, N.A., and McCormack, M.P. (2017). Hhex regulates hematopoietic stem cell self-renewal and stress hematopoiesis via repression of Cdkn2a. Stem Cells *35*, 1948–1957.

Janbandhu, V.C., Moik, D., and Fässler, R. (2014). Cre recombinase induces DNA damage and tetraploidy in the absence of loxP sites. Cell Cycle *13*, 462–470.

Jeevan-Raj, B., Gehrig, J., Charmoy, M., Chennupati, V., Grandclément, C., Angelino, P., Delorenzi, M., and Held, W. (2017). The transcription factor Tcf1 contributes to normal NK cell development and function by limiting the expression of granzymes. Cell Rep. *20*, 613–626.

Jung, H., Hsiung, B., Pestal, K., Procyk, E., and Raulet, D.H. (2012). RAE-1 ligands for the NKG2D receptor are regulated by E2F transcription factors, which control cell cycle entry. J. Exp. Med. *209*, 2409–2422.

Keng, V.W., Fujimori, K.E., Myint, Z., Tamamaki, N., Nojyo, Y., and Noguchi, T. (1998). Expression of Hex mRNA in early murine postimplantation embryo development. FEBS Lett. *426*, 183–186.

Keng, V.W., Yagi, H., Ikawa, M., Nagano, T., Myint, Z., Yamada, K., Tanaka, T., Sato, A., Muramatsu, I., Okabe, M., et al. (2000). Homeobox gene Hex is essential for onset of mouse embryonic liver development and differentiation of the monocyte lineage. Biochem. Biophys. Res. Commun. *276*, 1155–1161.

Kennedy, M.K., Glaccum, M., Brown, S.N., Butz, E.A., Viney, J.L., Embers, M., Matsuki, N., Charrier, K., Sedger, L., Willis, C.R., et al. (2000). Reversible defects in natural killer and memory CD8 T cell lineages in interleukin 15-deficient mice. J. Exp. Med. *191*, 771–780.

Kim, S., Iizuka, K., Kang, H.-S.P., Dokun, A., French, A.R., Greco, S., and Yokoyama, W.M. (2002). In vivo developmental stages in murine natural killer cell maturation. Nat. Immunol. *3*, 523–528.

Kostrzewski, T., Borg, A.J., Meng, Y., Filipovic, I., Male, V., Wack, A., DiMaggio, P.A., and Brady, H.J.M. (2018). Multiple levels of control determine how E4bp4/Nfil3 regulates NK cell development. J. Immunol. *200*, 1370–1381.

Kubo, A., Chen, V., Kennedy, M., Zahradka, E., Daley, G.Q., and Keller, G. (2005). The homeobox gene HEX regulates proliferation and differentiation of hemangioblasts and endothelial cells during ES cell differentiation. Blood *105*, 4590–4597.

Kühn, R., Schwenk, F., Aguet, M., and Rajewsky, K. (1995). Inducible gene targeting in mice. Science *269*, 1427–1429.

Liao, Y., Smyth, G.K., and Shi, W. (2014). featureCounts: an efficient general purpose program for assigning sequence reads to genomic features. Bioinformatics *30*, 923–930.

Lin, J.X., Migone, T.S., Tsang, M., Friedmann, M., Weatherbee, J.A., Zhou, L., Yamauchi, A., Bloom, E.T., Mietz, J., John, S., et al. (1995). The role of shared receptor motifs and common Stat proteins in the generation of cytokine pleiotropy and redundancy by IL-2, IL-4, IL-7, IL-13, and IL-15. Immunity *2*, 331–339.

Loftus, R.M., Assmann, N., Kedia-Mehta, N., O'Brien, K.L., Garcia, A., Gillespie, C., Hukelmann, J.L., Oefner, P.J., Lamond, A.I., Gardiner, C.M., et al. (2018). Amino acid-dependent cMyc expression is essential for NK cell metabolic and functional responses in mice. Nat. Commun. *9*, 2341.

Loonstra, A., Vooijs, M., Beverloo, H.B., Allak, B.A., van Drunen, E., Kanaar, R., Berns, A., and Jonkers, J. (2001). Growth inhibition and DNA damage induced by Cre recombinase in mammalian cells. Proc. Natl. Acad. Sci. U S A *98*, 9209–9214.

Madera, S., Geary, C.D., Lau, C.M., Pikovskaya, O., Reiner, S.L., and Sun, J.C. (2018). Cutting Edge: Divergent requirement of T-box transcription factors in effector and memory NK cells. J. Immunol. *200*, 1977–1981.

Marçais, A., Viel, S., Grau, M., Henry, T., Marvel, J., and Walzer, T. (2013). Regulation of mouse NK cell development and function by cytokines. Front. Immunol. *4*, 450.

Martinez Barbera, J.P., Clements, M., Thomas, P., Rodriguez, T., Meloy, D., Kioussis, D., and Beddington, R.S. (2000). The homeobox gene Hex is required in definitive endodermal tissues for normal forebrain, liver and thyroid formation. Development *127*, 2433–2445.

Martins, J.P., Andoniou, C.E., Fleming, P., Kuns, R.D., Schuster, I.S., Voigt, V., Daly, S., Varelias, A., Tey, S.-K., Degli-Esposti, M.A., and Hill, G.R. (2019). Strain-specific antibody therapy prevents cytomegalovirus reactivation after transplantation. Science *363*, 288–293.

Min-Oo, G., Bezman, N.A., Madera, S., Sun, J.C., and Lanier, L.L. (2014). Proapoptotic Bim regulates antigen-specific NK cell contraction and the generation of the memory NK cell pool after cytomegalovirus infection. J. Exp. Med. *211*, 1289–1296.

Mishra, A., Sullivan, L., and Caligiuri, M.A. (2014). Molecular pathways: interleukin-15 signaling in health and in cancer. Clin. Cancer Res. *20*, 2044–2050.

Morvan, M.G., and Lanier, L.L. (2016). NK cells and cancer: you can teach innate cells new tricks. Nat. Rev. Cancer *16*, 7–19.

Narni-Mancinelli, E., Chaix, J., Fenis, A., Kerdiles, Y.M., Yessaad, N., Reynders, A., Gregoire, C., Luche, H., Ugolini, S., Tomasello, E., et al. (2011). Fate mapping analysis of lymphoid cells expressing the NKp46 cell surface receptor. Proc. Natl. Acad. Sci. U S A *108*, 18324–18329.

Neri, S., Mariani, E., Meneghetti, A., Cattini, L., and Facchini, A. (2001). Calcein-acetyoxymethyl cytotoxicity assay: standardization of a method allowing additional analyses on recovered effector cells and supernatants. Clin. Diagn. Lab. Immunol. *8*, 1131–1135.

Ng, S.S., Souza-Fonseca-Guimaraes, F., Rivera, F.L., Amante, F.H., Kumar, R., Gao, Y., Sheel, M., Beattie, L., Montes de Oca, M., Guillerey, C., et al. (2018). Rapid loss of group 1 innate lymphoid cells during blood stage *Plasmodium* infection. Clin. Transl. Immunology *7*, e1003.

Nicholson, D.W., Ali, A., Thornberry, N.A., Vaillancourt, J.P., Ding, C.K., Gallant, M., Gareau, Y., Griffin, P.R., Labelle, M., Lazebnik, Y.A., et al. (1995). Identification and inhibition of the ICE/CED-3 protease necessary for mammalian apoptosis. Nature *376*, 37–43.

Noguchi, M., Nakamura, Y., Russell, S.M., Ziegler, S.F., Tsang, M., Cao, X., and Leonard, W.J. (1993). Interleukin-2 receptor gamma chain: a functional component of the interleukin-7 receptor. Science *262*, 1877–1880.

O'Sullivan, T.E. (2019). Dazed and confused: NK cells. Front. Immunol. *10*, 2235.

Ogilvy, S., Metcalf, D., Print, C.G., Bath, M.L., Harris, A.W., and Adams, J.M. (1999). Constitutive Bcl-2 expression throughout the hematopoietic compartment affects multiple lineages and enhances progenitor cell survival. Proc. Natl. Acad. Sci. U S A *96*, 14943–14948.

Ohs, I., van den Broek, M., Nussbaum, K., Münz, C., Arnold, S.J., Quezada, S.A., Tugues, S., and Becher, B. (2016). Interleukin-12 bypasses common gamma-chain signalling in emergency natural killer cell lymphopoiesis. Nat. Commun. *7*, 13708.

Osinalde, N., Sanchez-Quiles, V., Akimov, V., Guerra, B., Blagoev, B., and Kratchmarova, I. (2015). Simultaneous dissection and comparison of IL-2 and IL-15 signaling pathways by global quantitative phosphoproteomics. Proteomics *15*, 520–531.

Paz, H., Lynch, M.R., Bogue, C.W., and Gasson, J.C. (2010). The homeobox gene Hhex regulates the earliest stages of definitive hematopoiesis. Blood *116*, 1254–1262.

Rautela, J., Dagley, L.F., de Oliveira, C.C., Schuster, I.S., Hediyeh-Zadeh, S., Delconte, R.B., Cursons, J., Hennessy, R., Hutchinson, D.S., Harrison, C., et al. (2019). Therapeutic blockade of activin-A improves NK cell function and antitumor immunity. Sci. Signal. *12*, 596.

Ritchie, M.E., Phipson, B., Wu, D., Hu, Y., Law, C.W., Shi, W., and Smyth, G.K. (2015). limma powers differential expression analyses for RNA-sequencing and microarray studies. Nucleic Acids Res. *43*, e47.

Robinette, M.L., Fuchs, A., Cortez, V.S., Lee, J.S., Wang, Y., Durum, S.K., Gilfillan, S., and Colonna, M.; Immunological Genome Consortium (2015). Transcriptional programs define molecular characteristics of innate lymphoid cell classes and subsets. Nat. Immunol. *16*, 306–317.

Robinson, M.D., McCarthy, D.J., and Smyth, G.K. (2010). edgeR: a Bioconductor package for differential expression analysis of digital gene expression data. Bioinformatics *26*, 139–140.

Sathe, P., Delconte, R.B., Souza-Fonseca-Guimaraes, F., Seillet, C., Chopin, M., Vandenberg, C.J., Rankin, L.C., Mielke, L.A., Vikstrom, I., Kolesnik, T.B., et al. (2014). Innate immunodeficiency following genetic ablation of Mcl1 in natural killer cells. Nat. Commun. *5*, 4539.

Seillet, C., Belz, G.T., and Huntington, N.D. (2016). Development, homeostasis, and heterogeneity of NK Cells and ILC1. Curr. Top. Microbiol. Immunol. *395*, 37–61.

Skene, P.J., and Henikoff, S. (2017). An efficient targeted nuclease strategy for high-resolution mapping of DNA binding sites. eLife *6*, 576.

Slee, E.A., Harte, M.T., Kluck, R.M., Wolf, B.B., Casiano, C.A., Newmeyer, D.D., Wang, H.-G., Reed, J.C., Nicholson, D.W., Alnemri, E.S., et al. (1999). Ordering the cytochrome c-initiated caspase cascade: hierarchical activation of caspases-2, -3, -6, -7, -8, and -10 in a caspase-9-dependent manner. J. Cell Biol. *144*, 281–292.

Smith, H.R.C., Heusel, J.W., Mehta, I.K., Kim, S., Dorner, B.G., Naidenko, O.V., Iizuka, K., Furukawa, H., Beckman, D.L., Pingel, J.T., et al. (2002). Recognition of a virus-encoded ligand by a natural killer cell activation receptor. Proc. Natl. Acad. Sci. U S A *99*, 8826–8831.

Soufi, A., Smith, C., Clarke, A.R., Gaston, K., and Jayaraman, P.-S. (2006). Oligomerisation of the developmental regulator proline rich homeodomain (PRH/Hex) is mediated by a novel proline-rich dimerisation domain. J. Mol. Biol. *358*, 943–962.

Sugamura, K., Asao, H., Kondo, M., Tanaka, N., Ishii, N., Nakamura, M., and Takeshita, T. (1995). The common gamma-chain for multiple cytokine receptors. Adv. Immunol. *59*, 225–277.

Sun, J.C. (2016). Transcriptional control of NK cells. Curr. Top. Microbiol. Immunol. *395*, 1–36.

Sun, J.C., Ma, A., and Lanier, L.L. (2009). Cutting edge: IL-15-independent NK cell response to mouse cytomegalovirus infection. J. Immunol. *183*, 2911–2914.

Thomas, P.Q., Brown, A., and Beddington, R.S. (1998). Hex: a homeobox gene revealing peri-implantation asymmetry in the mouse embryo and an early transient marker of endothelial cell precursors. Development *125*, 85–94.

Viant, C., Guia, S., Hennessy, R.J., Rautela, J., Pham, K., Bernat, C., Goh, W., Jiao, Y., Delconte, R., Roger, M., et al. (2017). Cell cycle progression dictates the requirement for BCL2 in natural killer cell survival. J. Exp. Med. *214*, 491–510.

Wang, Y., Dong, W., Zhang, Y., Caligiuri, M.A., and Yu, J. (2018). Dependence of innate lymphoid cell 1 development on NKp46. PLoS Biol. *16*, e2004867.

Weizman, O.-E., Adams, N.M., Schuster, I.S., Krishna, C., Pritykin, Y., Lau, C., Degli-Esposti, M.A., Leslie, C.S., Sun, J.C., and O'Sullivan, T.E. (2017). ILC1 confer early host protection at initial sites of viral infection. Cell *171*, 795–808.e12.

Yang, M., Chen, S., Du, J., He, J., Wang, Y., Li, Z., Liu, G., Peng, W., Zeng, X., Li, D., et al. (2016). NK cell development requires Tsc1-dependent negative regulation of IL-15-triggered mTORC1 activation. Nat. Commun. *7*, 12730.

Zook, E.C., Li, Z.-Y., Xu, Y., de Pooter, R.F., Verykokakis, M., Beaulieu, A., Lasorella, A., Maienschein-Cline, M., Sun, J.C., Sigvardsson, M., and Kee, B.L. (2018). Transcription factor ID2 prevents E proteins from enforcing a naïve T lymphocyte gene program during NK cell development. Sci. Immunol. *3*, 22.

STAR★METHODS

KEY RESOURCES TABLE

REAGENT or RESOURCE	SOURCE	IDENTIFIER
Antibodies		
FcR blocking reagent	Miltenyi Biotec	Cat# 130-092-575
Armenian hamster anti-mouse CD3e (Clone 145-2C11)	BioLegend	Cat# 100302, RRID:AB_312667
Rat anti-mouse CD4 (Clone GK1.5)	BioLegend	Cat# 100402, RRID:AB_312687
Rat anti-mouse CD8a (Clone 53-6.7)	BioLegend	Cat# 100702, RRID:AB_3127414
Rat anti-mouse CD19 (Clone 6D5)	BioLegend	Cat# 115502, RRID:AB_313637
Rat anti-mouse F4/80 (Clone BM8)	BioLegend	Cat# 123102, RRID:AB_893506
Rat anti-mouse Ly6G (Clone 1A8)	BioLegend	Cat# 127602, RRID:AB_1089180)
Rat anti-mouse I-A/I-E (Clone M5/114.15.2)	BioLegend	Cat# 107602, RRID:AB_313317)
Rat anti-mouse TER-119 (Clone TER-119)	BD Biosciences	Cat# 553672, RRID:AB_394985
Rat anti-mouse MCL1 (Clone 19C4-15)	WEHI monoclonal antibody facility	N/A
Rat anti-mouse CD16/CD32 (Clone 2.4G2)	WEHI monoclonal antibody facility	N/A
Mouse anti-mouse BCL2 (Clone 10C4)	BioLegend	Cat# 633508, RRID:AB_2290367
Rat anti-mouse BIM (Clone 3C5)	WEHI monoclonal antibody facility	N/A
Rat anti-mouse EOMES (Clone Dan11mag)	Thermo Fisher Scientific	Cat# 46-4875-82, RRID:AB_10597455
Rat anti-mouse IFN-γ (Clone XMG1.2)	BD Biosciences	Cat# 554413, RRID:AB_398551
Mouse anti-human Ki-67 (Clone B56)	BD Biosciences	Cat# 556026, RRID:AB_396302
Mouse anti-mouse pSTAT5 (Y694)	BD Biosciences	Cat# 612567, RRID:AB_399858
Mouse anti-mouse β-actin (Clone AC-74)	Sigma-Aldrich	Cat# A2228, RRID:AB_476697
Armenian hamster anti-mouse CD3e (Clone 145-2C11)	BD Biosciences	Cat# 551163, RRID:AB_394082
Rat anti-mouse CD3e (Clone KT3-1.1)	WEHI monoclonal antibody facility	N/A
Rat anti-mouse CD3 (Clone 17A2)	BD Biosciences	Cat# 740147, RRID:AB_2739902)
Rat anti-mouse CD3 (Clone 17A2)	BioLegend	Cat# 100232, RRID:AB_2562554
Rat anti-mouse CD11b (Clone M1/70)	BD Biosciences	Cat# 740147, RRID:AB_2739902)
Rat anti-mouse CD11b (Clone M1/70)	BioLegend	Cat# 101257, RRID:AB_2565431
Rat anti-mouse CD11b (Clone M1/70)	WEHI monoclonal antibody facility	N/A
Armenian hamster anti-mouse CD27 (Clone LG.7F9)	BD Biosciences	Cat# 558754, RRID:AB_397106)
Armenian hamster anti-mouse CD27 (Clone LG.7F9)	BioLegend	Cat# 124229, RRID:AB_2565795
Armenian hamster anti-mouse CD27 (Clone LG.7F9)	Thermo Fisher Scientific	Cat# 47-0271-82, RRID:AB_10853642
Rat anti-mouse CD45 (Clone 30-F11)	BD Biosciences	Cat# 557659, RRID:AB_396774
Rat anti-mouse CD45 (Clone 30-F11)	BioLegend	Cat# 103134, RRID:AB_2562559
Mouse anti-mouse CD45.1 (Clone A20)	BD Biosciences	Cat# 560580, RRID:AB_1727489
Mouse anti-mouse CD45.1 (Clone A20)	Thermo Fisher Scientific	Cat# 11-0453-82, RRID:AB_465058)
Mouse anti-mouse CD45.2 (Clone 104)	BD Biosciences	Cat# 560694, RRID:AB_1727492)
Mouse anti-mouse CD45.2 (Clone 104)	BioLegend	Cat# 109839, RRID:AB_2562604
Armenian hamster anti-mouse CD49a (Clone Ha31/8)	BD Biosciences	Cat# 564863, RRID:AB_2738987)
Rat anti-mouse CD49b (Clone DX5)	BD Biosciences	Cat# 553857, RRID:AB_395093
Rat anti-mouse CD62L (Clone MEL-14)	Thermo Fisher Scientific	Cat# 25-0621-82, RRID:AB_469633)
Rat anti-mouse CD107a (Clone 1D4B)	BD Biosciences	Cat# 560648, RRID:AB_1727420

(*Continued on next page*)

Continued

REAGENT or RESOURCE	SOURCE	IDENTIFIER
Rat anti-mouse CD200R (Clone OX-110)	BioLegend	Cat# 123909, RRID:AB_1227748)
Rat anti-mouse DNAM-1 (Clone 10E5)	Thermo Fisher Scientific	Cat# 17-2261-82, RRID:AB_11149875
Rat anti-mouse DNAM-1 (Clone 10E5)	BioLegend	Cat# 128822, RRID:AB_2728146
Goat Anti-Rabbit IgG (HRP)	Abcam	Cat# ab97051, RRID:AB_10679369
Goat Anti-Mouse IgG (HRP)	Southern Biotech	Cat# 1070-05, RRID:AB_2650509
Rabbit anti-mouse HHEX (Clone 2018B)	R&D Systems	Cat# MAB83771, RRID:N/A
Rabbit anti-mouse HHEX (polyclonal)	Abcam	Cat# ab34222, RRID:N/A
Syrian hamster anti-mouse KLRG1 (Clone 2F1)	BD Biosciences	Cat# 564014, RRID:AB_2738542
Syrian hamster anti-mouse KLRG1 (Clone 2F1)	Thermo Fisher Scientific	Cat# 25-5893-82, RRID:AB_1518768
Mouse anti-mouse Ly49A (Clone A1)	Thermo Fisher Scientific	Cat# 12-5856-82, RRID:AB_1311270
Mouse anti-mouse Ly49C/I (Clone 5E6)	BD Biosciences	Cat# 553277, RRID:AB_394751
Rat anti-mouse Ly49D (Clone 4E5)	BD Biosciences	Cat# 555313, RRID:AB_395724)
Rat anti-mouse Ly49D (Clone 4E5)	BioLegend	Cat# 138302, RRID:AB_10574460
Rat anti-mouse Ly49G2 (Clone 4D11)	BD Biosciences	Cat# 555315, RRID:AB_395726
Mouse anti-mouse Ly49H (Clone 3D10)	Thermo Fisher Scientific	Cat# 17-5886-82, RRID:AB_10598809
Mouse anti-mouse Ly49H (Clone 3D10)	BioLegend	Cat# 144702, RRID:AB_2561549
Mouse anti-mouse NK1.1 (Clone PK136)	BD Biosciences	Cat# 564143, RRID:AB_2738617
Mouse anti-mouse NK1.1 (Clone PK136)	WEHI monoclonal antibody facility	N/A
Rat anti-mouse NKG2D (Clone CX5)	BD Biosciences	Cat# 558403, RRID:AB_647201
Rat anti-mouse NKG2D (Clone CX5)	BioLegend	Cat# 130202, RRID:AB_1227717
Rat anti-mouse NKp46 (Clone 29A1.4)	BD Biosciences	Cat# 560757, RRID:AB_1727466
Rat anti-mouse NKp46 (Clone 29A1.4)	BioLegend	Cat# 137611, RRID:AB_10915472
Rat anti-mouse NKp46 (Clone 29A1.4)	BioLegend	Cat# 137602, RRID:AB_10552740
Rat anti-mouse NKp46 (Clone 29A1.4)	Thermo Fisher Scientific	Cat# 25-3351-82, RRID:AB_2573442
Armenian hamster anti-mouse TCRβ (Clone H57-597)	BD Biosciences	Cat# 560657, RRID:AB_1727575
Armenian hamster anti-mouse TCRβ (Clone H57-597)	BioLegend	Cat# 109212, RRID:AB_313435
Armenian hamster anti-mouse TCRβ (Clone H57-597)	WEHI monoclonal antibody facility	N/A
Chemicals, Peptides and Recombinant Proteins		
20X Bolt MOPS SDS Running Buffer	Thermo Fisher Scientific	Cat# B0001
4X Bolt LDS Sample Buffer	Thermo Fisher Scientific	Cat# B0007
10X Bolt Sample Reducing Agent	Thermo Fisher Scientific	Cat# B0009
Calcein-AM	BD Biosciences	Cat# 564061
CellTrace Violet	Thermo Fisher Scientific	Cat# C34557
Clarity Western ECL substrate	Bio-Rad	Cat# 1705061
Collagenase Type 4	Worthington	Cat# LS004188
DNase-1	Worthington	Cat# LS002139
Fixable Viability Stain 510	BD Biosciences	Cat# 564406
Fixable Viability Stain 780	BD Biosciences	Cat# 565388
GolgiStop	BD Biosciences	Cat# 554724
Ionomycin	Merck	Cat# I0634
Lyse/Fix buffer 5X	BD Biosciences	Cat# 558049
Mouse IL-12	Miltenyi Biotec	Cat# 130-096-708
Neomycin sulfate	Sigma-Aldrich	Cat# N1876
Percoll	GE Healthcare	Cat# 17-0891-01

(*Continued on next page*)

Continued

REAGENT or RESOURCE	SOURCE	IDENTIFIER
Perm buffer III	BD Biosciences	Cat# 558050
PMA	Merck	Cat# P8139
Poly(I:C)	Merck	Cat# P1530
Recombinant human IL-15	Miltenyi Biotec	Cat# 130-095-766
Recombinant human IL-18	MBL International	Cat# B001-5
RIPA lysis buffer 10X	Merck	Cat# 20-188
Stain buffer (FBS)	BD Biosciences	Cat# 554656
Sytox Blue	Thermo Fisher Scientific	Cat# S34857
Zombie UV Fixable Viability Kit	BioLegend	Cat# 423108
Critical Commercial Assays		
CellEvent Caspase-3/7 Flow Cytometry Assay Kit	Thermo Fisher Scientific	Cat# C10427
Click-iT Plus EdU Alexa Fluor 488 Flow Cytometry Assay Kit	Thermo Fisher Scientific	Cat# C10633
EasySep Mouse NK Isolation Kit	StemCell Technologies	Cat# 19855
Foxp3 Staining Buffer Set Kit	Thermo Fisher Scientific	Cat# 00-5523-00
MGIEasy DNA FS Library Prep Set	MGITech	Cat# 1000017572
NEBNext Ultra II Directional RNA Library Prep Kit for Illumina	New England Biolabs	Cat# E7760L
RNeasy Plus Mini Kit	QIAGEN	Cat# 74134
Deposited Data		
RNA-sequencing on bulk $CD3^{-}NK1.1^{+}NKp46^{+}CD49b^{+}$ *Hhex*$^{\Delta/\Delta}$ and *Cre* control NK cells	This paper	GEO database accession number GEO: GSE140284
CUT&RUN-sequencing on cultured C57BL/6 WT NK cells	This paper	GEO database accession number GEO: GSE155957
Experimental Models: Cell Lines		
Mouse: B16F10 melanoma	ATCC	Cat# CRL-6475, RRID:CVCL_0159
Experimental Models: Organisms/Strains		
Mouse: *Bcl2*$^{T/+}$	Ogilvy et al., 1999	N/A
Mouse: *Bim*$^{fl/fl}$	Herold et al., 2014	N/A
Mouse: CD45.1 congenic	WEHI Bioservices	N/A
Mouse: ca*Stat5*$^{T/+}$	Burchill et al., 2003	N/A
Mouse: F1 (CD45.1/CD45.2)	WEHI Bioservices	N/A
Mouse: *Hhex*$^{fl/fl}$	Hunter et al., 2007	N/A
Mouse: *Hhex*$^{-/fl}$	Bogue et al., 2003	N/A
Mouse: *Hhex*$^{fl/fl}$*Bim*$^{fl/fl}$	This paper	N/A
Mouse: IL-15 Tg	Fehniger et al., 2001	N/A
Mouse: *Mx1-Cre*	Kühn et al., 1995	N/A
Mouse: *Ncr1*^{iCre}	Narni-Mancinelli et al., 2011	N/A
Software and Algorithms		
FlowJo 10.6.1	FlowJo	N/A
GraphPad Prism 8	GraphPad	N/A
R Studio	https://rstudio.com/	N/A
Virus strains		
MCMV strain K181-Perth	Martins et al., 2019	N/A
Other		
123count eBeads	Thermo Fisher Scientific	Cat# 01-1234-42
MagniSort Streptavidin Negative Selection Beads	Thermo Fisher Scientific	Cat# MSNB-6002-74

RESOURCE AVAILABILITY

Lead Contact

Further information and requests for resources and reagents should be directed to and will be fulfilled by the lead contact, Nicholas D. Huntington (nicholas.huntington@monash.edu.au).

Materials Availability

This study did not generate new unique reagents.

Data and Code Availability

The RNA-seq and CnR-seq data generated in this study are available on GEO database (accession number GEO: GSE140284 and GEO: GSE155957, respectively).

EXPERIMENTAL MODEL AND SUBJECT DETAILS

Mice

The mouse strains *Hhex*$^{fl/fl}$ (Hunter et al., 2007), *Hhex*$^{-/fl}$ (Bogue et al., 2003), *Ncr1*^{Cre} (Narni-Mancinelli et al., 2011), *Bim*$^{fl/fl}$ (Herold et al., 2014), ca*Stat5b*$^{T/+}$ (Burchill et al., 2003), *Bcl2*$^{T/+}$ (Ogilvy et al., 1999), IL-15 Tg (Fehniger et al., 2001) and *Mx1-Cre* (Kühn et al., 1995) have been described. *Hhex*$^{fl/fl}$ mice were crossed with *Ncr1*^{Cre} mice to generate *Hhex*$^{fl/fl}$*Ncr1*$^{+/Cre}$ mice (*Hhex*$^{\Delta/\Delta}$). *Hhex*$^{\Delta/\Delta}$ mice were crossed with *Bim*$^{fl/fl}$ mice to generate *Hhex*$^{\Delta/\Delta}$*Bim*$^{\Delta/\Delta}$ mice. Crossings between *Hhex*$^{-/fl}$, ca*Stat5b*$^{T/+}$, *Bcl2*$^{T/+}$ and *Mx1-Cre* mice were carried out to generate *Hhex*$^{-/fl}$, *Hhex*$^{-/fl}$ca*Stat5b*$^{T/+}$, and *Hhex*$^{-/fl}$*Bcl2*$^{T/+}$ mice. Systemic deletion of *Hhex* in these mice to generate *Hhex*$^{-/\Delta}$, *Hhex*$^{-/\Delta}$ca*Stat5b*$^{T/+}$, and *Hhex*$^{-/\Delta}$*Bcl2*$^{T/+}$ mice was induced by intraperitoneally (i.p.) administering 7 week old mice with three 200 mg/kg doses of polyinosinic-polycytidylic acid sodium salt (poly(I:C); Merck Cat# P1530) dissolved in sterile saline, every other day. Crossings between *Hhex*$^{+/+}$, *Hhex*$^{fl/fl}$, *Bcl2*$^{T/+}$ and ca*Stat5*$^{T/+}$ mice were carried out to generate *Hhex*$^{+/fl}$, ca*Stat5b*$^{T/+}$*Hhex*$^{+/fl}$, and *Bcl2*$^{T/+}$*Hhex*$^{+/fl}$ control mice. Mice on a congenic CD45.1 background or F1 background between CD45.1 and CD45.2 were sourced from WEHI Bioservices and used as control donors (wild-type; WT) in chimeric studies. *Ncr1*$^{+/Cre}$ mice (*Cre* control) were used as controls for *Hhex*$^{\Delta/\Delta}$ mice and to account for *Cre* recombinase-associated toxicity (Loonstra et al., 2001; Janbandhu et al., 2014). All genetically modified mouse strains used in this study were either maintained on a C57BL/6 background or have been backcrossed for > 10 generations to C57BL/6. Both male and female mice aged between 8 to 16 weeks were used for experiments. Animal experiments performed were carried out in accordance with the National Health and Medical Research Committee (NHMRC) *Australian code of practice for the care and use of animals for scientific purposes* and approved by the WEHI Animal Ethics Committee.

Cells

Purified NK cells were maintained in Iscove's Modified Dulbecco's Medium (IMDM) supplemented with 10% (v/v) fetal bovine serum (FBS), 2 mM GlutaMAX (GIBCO Cat# 35050), 50 μM β-mercaptoethanol (β-ME, Sigma-Aldrich Cat# M6250), 50 ng/ml recombinant hIL-15 (rhIL-15; Miltenyi Biotec Cat# 130-095-766), 100 μg/ml streptomycin and 100 IU/ml penicillin (Sigma-Aldrich Cat# P0781). The murine B16F10 melanoma cell line (ATCC Cat# CRL-6475) was maintained in Dulbecco's Modified Eagles Medium (DMEM) containing 10% (v/v) FBS, 50 μM β-ME, 100 μg/ml streptomycin and 100 IU/ml penicillin. All cells were maintained in a humidified incubator at 37°C with 5% CO_2.

Viruses

The murine cytomegalovirus (MCMV) used in this study is from salivary gland-propagated stocks of the virulent MCMV strain K181-Perth (Martins et al., 2019).

METHOD DETAILS

Bone marrow chimeras

CD45.2 (IL-15 Tg and WT) recipient mice were exposed twice, 3 hours apart, to 5.5 Gray (Gy) gamma-irradiation from a ^{60}Co source. CD45.1 recipient mice received a single dose of 9.5 Gy from a ^{137}Cs source. Irradiated mice were injected intravenously (i.v.) with a 50:50 mixture of live nucleated cells from control and experimental donors. *Hhex*$^{-/\Delta}$, *Hhex*$^{-/\Delta}$ca*Stat5b*$^{T/+}$, and *Hhex*$^{-/\Delta}$*Bcl2*$^{T/+}$ experimental donors were used at least 4 weeks after poly(I:C) (Merck Cat# P1530) treatment. All recipient mice were maintained on oral neomycin-sulfate (2 mg/ml; Sigma-Aldrich Cat# 1876) for 3 weeks post-transplantation. Hematopoietic and NK cell reconstitution was assessed at least 6 weeks post-transplantation.

Flow cytometry and cell sorting

Spleens, bone marrows, lungs and livers were processed differently to obtain single cell suspensions. Spleens and livers were passed through 70 μm filters. Bone marrow flushed from a femur and tibia were repeatedly passed through a needle to disaggregate

cells. Lungs were minced and enzymatically digested with 1 mg/ml Collagenase Type 4 (Worthington Cat# LS004188) and 30 μg/ml DNase-1 (Worthington Cat# LS002139) in PBS. Digested lungs were passed through 70 μm filters to disaggregate remaining cell clumps. Dissociated livers and lungs were further subjected to isopycnic centrifugation in 33.75% v/v isotonic Percoll (GE Healthcare Cat# 17-0891-01) to remove parenchymal cells. RBCs were cleared from all dissociated tissues by osmotic lysis.

Single cell suspensions were stained with monoclonal antibodies (Thermo Fisher Scientific, BD Biosciences and BioLegend) against CD3 (17A2 or 145-2C11), CD11b (M1/70), CD27 (LG.7F9), CD45 (30-F11), CD45.1 (A20), CD45.2 (104), CD49a (Ha31/8), CD49b (DX5), CD62L (MEL-14), CD107a (1D4B), CD122 (TM-β1), CD200R (OX-110), DNAM-1 (10E5), KLRG1 (2F1), Ly49A (A1), Ly49C/I (5E6), Ly49D (4E5), Ly49G2 (4D11), Ly49H (3D10), NK1.1 (PK136), NKG2D (CX5), NKp46 (29A1.4), TCRß (H57-597), BCL2 (10C4), BIM (3C5), EOMES (Dan11mag), IFN-γ (XMG1.2), Ki-67 (B56), MCL1 (19C4-15), phospho-STAT5 (pSTAT5; 47) in the presence of CD16/32 (2.4G2). Propidium iodide (PI; 50 ng/ml), 500 nM SYTOX Blue (Thermo Fisher Scientific Cat# S34857), Fixable Viability Stain 510 (FVS510; BD Biosciences Cat# 564406) or FVS780 (BD Biosciences Cat# 565388) were used to exclude dead cells. Detection of activated caspase-3/7 in apoptotic cells was performed with a CellEvent Caspase-3/7 Flow Cytometry Assay Kit (Thermo Fisher Scientific Cat# C10427) according to the manufacturer's protocol. Cells numbers per organ were enumerated using 123count eBeads (Thermo FIsher Scientific Cat# 01-1234-42). Staining for intracellular antigens (BCL2, BIM, EOMES, IFN-γ, Ki-67 and MCL1) was performed using the Foxp3 Transcription Factor Staining Buffer Set (Thermo Fisher Scientific Cat# 00-5523-00). Intracellular staining for phosphorylated proteins (pSTAT5) was performed using Phosflow Lyse/Fix buffer (Cat# 558049) and Perm buffer III (Cat# 558050) from BD Biosciences. Cells were acquired on BD LSRFortessa X-20 and FACSVerse cell analyzers (BD Biosciences) and analysis was performed using FlowJo software (v10, TreeStar Inc.). The following pre-gating strategy was consistently applied in immunophenotyping analyses: single cell, viable, $CD45^+CD3^-NK1.1^+$.

Prior to sorting, splenic suspensions were enriched for NK cells by immunomagnetic bead depletion with the following biotinylated antibodies TER-119 (TER-119), F4/80 (BM8), Ly6G (1A8), CD3 (145-2C11), CD4 (GK1.5), CD8α (53-6.7), CD19 (6D5) and MHC II (M5/114.15.2) from BioLegend, MagniSort Streptavidin Negative Selection Beads (Thermo Fisher Scientific Cat# MSNB-6002-74) and an EasySep Magnet (StemCell Technologies). NK cells, sorted on single cell, viable, $CD45^+CD3^-CD19^-NK1.1^+NKp46^+CD49b^+$, were recovered from the enriched supernatant using FACSAria III and FACSAria Fusion cell sorters (BD Biosciences).

NK cell stimulation and proliferation

To track NK cell proliferation *in vitro*, freshly isolated NK cells were labeled with 5 μM CellTrace Violet (Thermo Fisher Scientific Cat# C34557) as described (Hennessy et al., 2019) and cultured with the indicated concentrations of recombinant human IL-15 (rhIL-15; Miltenyi Biotec Cat#130-095-766) for up to 120 h. Viable NK cells were enumerated using PI and 123count eBeads (Thermo FIsher Scientific Cat# 01-1234-42).

In STAT5 signaling studies, expanded NK cells were first starved of rhIL-15 for at least 4 h and then re-exposed to 50 ng/ml rhIL-15 (Miltenyi Biotec Cat#130-095-766). pSTAT5 levels were measured as described in 30 min intervals over 2 h.

For *in vitro* assessment of NK cell degranulation and IFN-γ production, splenic suspensions immunomagnetically depleted of RBCs were stimulated with either 20 ng/ml phorbol 12-myristate 13-acetate (PMA; Merck Cat# P8139) and 1 μg/ml ionomycin (Merck Cat# I0634) or 10 ng/ml mIL-12 (Miltenyi Biotec Cat# 130-096-708) and 100 ng/ml mIL-18 (MBL Cat# B001-5) for 4 h at 37°C to respectively induce NK cell degranulation or IFN-γ production. For plate-bound antibody stimulation, RBC-depleted splenocytes were first treated with mouse FcR blocking reagent (Miltenyi Biotec Cat# 130-092-575) and then incubated for 4 h at 37°C in corresponding wells that have been pre-coated with 5 μg/ml purified antibodies against DNAM-1 (10E5; Cat# 128822), Ly49D (4E5; Cat# 138302), Ly49H (3D10; Cat# 144702), NKG2D (CX5; Cat# 130202) and NKp46 (29A1.4; Cat# 137602) from BioLegend. All cells were stimulated in the presence of GolgiSTOP (BD Biosciences Cat# 554724), anti-CD107a (1D4B; BD Biosciences Cat# 560648) and 10-25 ng/ml rhIL-15 (Miltenyi Biotec Cat# 130-095-766).

Calcein release assay

NK cell cytotoxicity *in vitro* was assessed using the calcein release assay as described (Neri et al., 2001). Briefly, freshly sorted or cultured NK cells were suspended in assay medium; phenol-red free RPMI 1640 medium supplemented with 10% (v/v) FBS, 50 μM βME, 2 mM GlutaMAX, 1mM sodium pyruvate (GIBCO Cat# 11360-070), 25 mM HEPES (GIBCO Cat# 15630-080) and 1X MEM non-essential amino acids (NEAA) solutions (GIBCO Cat# 11140-050). B16F10 melanoma (ATCC Cat# CRL-6475) target cells labeled with 15 μM Calcein-AM (BD Biosciences Cat# 564061) were incubated with effector cells at the indicated effector to target (E:T) ratios for 4 h at 37°C. As controls, target cells were also incubated in assay medium in the absence of effector cells or 2% Triton X-100. Calcein release from target cells was quantified by measuring fluorescent emission (excitation filter: 485 ± 9 nm; cutoff: 515 nm; emission: 525 ± 15 nm) from 100 μl cell-free supernatant with an EnVision Multimode Plate Reader (Perkin Elmer).

Murine cytomegalovirus infection

Mice were injected i.p. with 10^4 plaque-forming units (PFU) of murine cytomegalovirus (MCMV). Control mice were mock infected with Mouse Osmolarity Buffered Saline (MOBS; 330 mOSm)/5% FBS. Mice were sacrificed at days 7 and 10 post-infection (p.i.) for immunophenotyping of $NKp46^+$ NK cells (spleen and liver) and determination of viral titers (spleen, salivary gland and lung) by plaque assays.

EdU incorporation assay

5-ethynyl-2′-deoxyuridine (EdU) incorporation was performed using a Click-iT Plus EdU Alexa Fluor 488 Flow Cytometry Assay Kit (Thermo Fisher Scientific Cat# C10633) according to the manufacturer's protocol, with exception to the amount of EdU and number of doses administered. Mice were injected i.p. with two doses of 200 μg EdU on alternating days. Control mice received sterile PBS under the same dosing regimen. Spleens were harvested 24 h after the 2nd injection and processed into single cell suspensions as described for subsequent EdU detection according to the manufacturer's protocol.

SDS polyacrylamide gel electrophoresis and western blotting

NK cell lysates were obtained by lysing NK cell pellets in 1X RIPA lysis buffer (Merck Cat# 20-188) containing 1X cOmplete Mini EDTA-free Protease Inhibitor Cocktail (Sigma-Aldrich, Cat# 11836170001). Lysates were clarified (16000 *g* for 10 min at 4°C) prior to protein quantification with a Pierce BCA Protein Assay Kit (Thermo Scientific Cat# 23227). 1X Bolt LDS Sample Buffer (Thermo Fisher Scientific Cat# B0007) and 1X Bolt Sample Reducing Agent (Thermo Fisher Scientific Cat# B0009) were added to lysates and boiled for 5 min at 95°C. Proteins within the lysates were resolved on Bolt 4%–12% Bis-Tris Plus (Thermo Fisher Scientific) precast polyacrylamide gels in 1X Bolt MOPS SDS Running Buffer (Thermo Fisher Scientific Cat# B0001). Separated proteins were dry blotted onto nitrocellulose membrane stacks (Thermo Fisher Scientific) using Program 0 (20 V for 1 min, 23 V for 4 min and 25 V for 2 min) on an iBlot2 Gel Transfer Device (Thermo Fisher Scientific). Membranes were blocked in PBS-T (PBS and 0.1% (v/v) Tween) containing 5% (w/v) skim milk powder before overnight incubation at 4°C with primary antibodies in PBS-T containing 5% (w/v) BSA and 0.05% (w/v) sodium azide. Primary antibodies used were HHEX rabbit monoclonal antibody (2018B; R&D Systems Cat# MAB83771) and β-actin mouse monoclonal antibody (AC-74; Sigma-Aldrich). Incubations with horseradish peroxidase (HRP)-conjugated secondary antibodies in PBS-T containing 5% (w/v) skim milk were allowed to proceed for 1h at room temperature. Secondary antibodies used were polyclonal goat anti-rabbit IgG H&L (Abcam Cat# ab97051) and polyclonal goat anti-mouse IgG (Southern Biotech Cat# 1070-05). Labeled proteins were visualized using Clarity Western Enhanced Chemiluminescence (ECL) substrate (Bio-Rad Cat# 1705061) and imaged using a ChemiDoc Imager (Bio-Rad).

RNA sequencing and data analysis

RNA isolation from sorted NK cells were extracted using a RNeasy Plus Mini Kit (QIAGEN Cat# 74134), according to the manufacturer's protocol. RNA samples were quantified using the Agilent 2200 TapeStation System (Agilent). Next-generation sequencing libraries were prepared with quality-controlled RNA samples (RIN > 7.0) from at least three biological replicates per genotype using an NEBNext Ultra II Directional RNA Library Prep Kit for Illumina (New England Biolabs Cat# E7760L). cDNA libraries were pooled and subjected to 75 bp single end sequencing at the WEHI Genomics Laboratory on a NextSeq 500 next-generation sequencer (Illumina) to obtain approximately 20 million reads per sample. Reads were aligned to mm10/GRCm38 Gencode version M16 (Ensembl 91) using the STAR (Dobin et al., 2013) aligner. Genewise counts were obtained using featureCounts (Liao et al., 2014). Genes with counts-per-million (CPM) greater than 0.5 in at least three biological replicates were retained in the downstream analysis. The gene expression values were TMM normalized (Robinson et al., 2010). Differentially expressed genes were determined by fitting a Quasi-likelihood Negative Binomial Generalized Log Linear model per gene using edgeR (Robinson et al., 2010). Genes were called differentially expressed if they achieved a false discovery rate of less than 0.05. Pathway enrichments and gene set tests were carried out using limma (Ritchie et al., 2015). ILC1 signature genes were derived from publicly available microarray data (Robinette et al., 2015; accession number GSE37488). RNA-sequencing data generated from *ex vivo* isolated *Cre* control and *Hhex*$^{\Delta/\Delta}$ NK cells was deposited into GEO database (accession number GSE140284).

CUT&RUN

NK cells from the spleen of one C57BL/6 (WT) mouse were enriched with the EasySep mouse NK isolation kit (StemCell Technologies Cat# 19855) according to the manufacturer's instructions and cultured for 5 days in the presence of 50 ng/ml rhIL-15. CUT&RUN (Skene and Henikoff, 2017) was performed with 500,000 freshly isolated nuclei using polyclonal rabbit anti-HHEX antibody (Abcam Cat# ab34222). Libraries were constructed using MGIEasy DNA FS library prep set 2 (MGITech Cat# 1000017572) and run on the MGITech MGISEQ2000RS platform using MGIEasy V3 chemistry with FCL flowcell according to the manufacturer's instructions. Data was demultiplexed using splitBarcode and trimmed to 100b using bbduk. Fastq files were aligned to mm10 using Bowtie2 and peaks were called using MACS2 over the control sample (without primary antibody). Data was visualized using IGV and deposited into GEO database (accession number GSE155957).

QUANTIFICATION AND STATISTICAL ANALYSIS

Statistical analyses were performed using GraphPad Prism v7 (GraphPad Software). The two-tailed Student's *t test* was used to test for significant differences ($p < 0.05$) between two samples with normally distributed parameters. Welch's correction was applied when the standard deviation between samples were unequal (F-test, $p < 0.05$). The Mann-Whitney test was used to test for significant differences ($p < 0.05$) between two samples with parameters that are not normally distributed. Exact *p values*, except when $p < 0.001$, are indicated in the figures and all error bars represent the standard deviations of the mean of the respective datasets.